arXiv:cond-mat/0502131v1 [cond-mat.other] 4 Feb 2005

Interplay of magnetic ordering and CEF anisotropy in the hexagonal compounds RPtIn, R = Y, Gd - Lu

E. Morosan, S. L. Bud'ko and P. C. Canfield
Ames Laboratory and Department of Physics and Astronomy, Iowa State University, Ames, IA 50011, USA
(Dated: February 2, 2008)

Single crystals of RPtIn, R = Y, Gd - Lu were grown out of In-rich ternary solution. Powder X-ray diffraction data on all of these compounds were consistent with the hexagonal ZrNiAl-type structure (space group P $\overline{6}$ 2 m). The R = Tb and Tm members of the series appear to order antiferromagnetically (T_N = 46.0 K, and 3.0 K respectively), whereas the R = Gd, Dy - Er compounds have at least a ferromagnetic component of the magnetization along the c-axis. The magnetic ordering temperatures of all of these systems seem to scale well with the de Gennes factor dG, whereas the curious switching from ferromagnetic to antiferromagnetic ordering across the series is correlated with a change in anisotropy, such that, in the low temperature paramagnetic state, $\chi_{ab} > \chi_c$ for the antiferromagnetic compounds, and $\chi_c > \chi_{ab}$ for the rest. In order to characterize the magnetic ordering across the RPtIn series, a three-dimensional model of the magnetic moments in Fe_2P-type systems was developed, using the *three co-planar Ising-like systems model* previously introduced for the extremely planar TbPtIn compound: given the orthorhombic point symmetry of the R sites, we assumed the magnetic moments to be confined to six non-planar easy axes, whose in-plane projections are rotate by 60^0 with respect to each other. Such a model is consistent with the reduced high-field magnetization values observed for the RPtIn compounds, R = Tb - Tm, and qualitatively reproduces the features of the angular dependent magnetization of $Ho_xY_{1-x}PtIn$ at H = 55 kG.

PACS numbers: 75.25.+z; 75.10.-b; 75.30.Gw; 75.30.Kz; 75.50.Ee

I. Introduction

The RPtIn compounds (R = Y, La-Sm, Gd-Lu) have been reported to crystallize in the ZrNiAl hexagonal structure[1,2,3], space group $P\overline{6}2m$, with the rare earth in orthorhombic point symmetry, whereas the R = Eu member of this series forms in an orthorhombic TiNiSi-type structure[4,5] (space group *Pnma*). Magnetic and transport measurements on some of these materials revealed a variety of physical properties across the series: CePtIn[6,7,8,9] and YbPtIn[10,11,12] appear to be dense Kondo systems, with the electronic specific heat coefficient γ larger than 500 mJ/mol K^2, and 430 mJ/mol K^2 respectively; no magnetic order was observed in the former compound down to 60 mK[9], whereas the latter appears to order antiferromagnetically below 3.4 K[10]. In TbPtIn[13] the antiferromagnetic nature of the magnetic order below 50 K was indirectly suggested by the metamagnetic transitions observed in the M(H) data below this temperature. Watson *et al.*[13] have also reported that the R = Gd and Dy members of this series have ferromagnetic ground states, with T_C = 89 K, and 38 K respectively, with reduced values of both the effective and the saturated moments of these two compounds. Whereas for the Dy system, the disagreement with the respective theoretical values could be attributed to crystal electric field CEF effects, it was unclear what was causing it in GdPtIn. CEF effects are also apparent in the magnetization measurements on PrPtIn down to T = 1.7 K, which, together with the resistivity data[2] suggest a possible ferromagnetic transition at lower temperatures. Similar data on SmPtIn are indicative of ferromagnetic ordering in this compound below T_C = 25 K.

We recently presented detailed magnetization and transport measurements on single crystals of TbPtIn[14]: anisotropic low-field susceptibility and specific heat measurements confirm the antiferromagnetic ground state, with T_N = 46 K, slightly different than the previously reported value[13]; below the ordering temperature, complex metamagnetism is revealed by magnetization measurements with applied field in the basal plane. Whereas from the high-temperature inverse susceptibility we obtained an effective moment μ_{eff} = 9.74 μ_B/Tb^{3+}, close to the theoretical value 9.72 μ_B, the high-field magnetization data yielded values only up to $\sim$ 6 μ_B/Tb^{3+}, much smaller than the theoretical saturated moment of 9 μ_B. In order to explain the reduced magnetization values, as well as the angular dependence of the metamagnetic properties, we proposed a *three co-planar Ising-like systems model*, which took into account the orthorhombic point symmetry of the rare earth ions in the hexagonal unit cell of the RPtIn compounds[14]. Within such a model, for applied magnetic fields far smaller than the CEF splitting energy, for TbPtIn one expects a crystal field limited saturated paramagnetic CL-SPM state equal to 6 μ_B.

In view of these existing magnetization and transport data, the magnetic ordering in the heavy rare earth members of the RPtIn series was somewhat intriguing: whereas for GdPtIn and DyPtIn, ferromagnetic ground states were reported, the intermediate R = Tb member appears to order antiferromagnetically, which is a rather unusual discontinuity for a magnetically ordering local moment series.

In the present work we are trying to address this problem, and also extend the characterization of the physical properties to all the heavy RPtIn systems (*i.e.*, for R = Y, Gd - Lu). Having been able to grow single crystals for all of these compounds, we have the possibility of determining the effect of the CEF anisotropy on their magnetic properties, more so than in the previous studies on polycrystalline samples. As we shall see, the hexagonal crystal structure of these compounds, with three R ions in the unit cell occupying unique orthorhombic point symmetry sites, is of crucial importance in explaining the moment configurations and magnetic ordering in the RPtIn materials described here.

In presenting our data, we will start with the non-magnetic members of the RPtIn series, R = Y and Lu; then we will continue with the magnetic ones (R = Gd - Tm), characterizing each of the compounds by temperature- and field-dependent magnetization, as well as zero-field specific heat measurements. A brief description of the previously reported[10,11,12] heavy fermion compound YbPtIn is also included, our measurements being performed, as with all the other R compounds, on solution-grown single crystals.

Next, we will briefly present the model for the magnetic moment configuration, characterizing the extremely planar TbPtIn compound (which is described in detail by Morosan *et al.*[14]); a more generalized version of this model, extended to three dimensions, will then be used to describe the magnetism in the other magnetic compounds except YbPtIn.

We will conclude by emphasizing the possibility of generalizing our *three co-planar Ising-like systems model* to a three dimensional one, which could potentially describe hexagonal systems with orthorhombic point symmetry of the rare earth site beyond the RPtIn series. Directions for further experiments which could potentially probe the validity of our assumed model will also be discussed.

II. EXPERIMENTAL METHODS

Single crystals of RPtIn (R = Y, Gd - Lu) were grown out of high-temperature ternary solution[14,15,16,17]. Initial concentrations used were typically $R_xPt_xIn_{1-2x}$, with $x = 0.05 - 0.10$, and the resulting crystals were well-formed hexagonal rods. The In-rich self-flux was used because it lowers the liquid-solidus surface of primary solidification for RPtIn, and also introduces no new elements into the melt. After placing the constituent elements in alumina crucibles, the crucibles were sealed in quartz ampoules under partial argon pressure. In most cases the ampoules were initially heated up to $\sim 1200^0$ C, and then slowly cooled down to $\sim 800^0$ C, over 50 to 100 hours. Subsequently, the excess liquid solution was decanted, and the resulting hexagonal rods were, if necessary, quickly etched in HCl to remove residual flux from the surface. Higher decanting temperatures (*i.e.*, above 1000^0 C) were necessary for R = Y, Gd and Er, whereas in the case of TmPtIn the temperature interval for which best crystals were obtained was lower (between 1100^0 C to 750^0 C). In some cases, the hexagonal rods had hollow channels in the center, sometimes with flux inclusions. We succeeded in optimizing the growth of TbPtIn by using faster cooling rates (*i.e.*, 400^0 C / 50h); this yielded only well-formed, full, hexagonal rods, whereas when slowing down the cooling process hollow crystals were obtained together with full, smaller ones. Slight modifications of the initial concentrations and/or growth profiles for Dy, Ho or Er didn't totally eliminate the formation of hollow rods, but 100 % dense samples could easily be found. For all our measurements, carefully chosen, well-formed single crystals were used, so as to avoid possible mass errors on hollow rods to propagate into our data.

A drastic modification of the growth procedure needed to be made for YbPtIn: a ternary solution with initial composition $Yb_{0.4}Pt_{0.1}In_{0.5}$ was sealed in a 3-cap Ta crucible[20], and slow-cooled from 1200^0 C to 1000^0 C over $\sim$ 100 hours, resulting in well-formed hexagonal rods.

To confirm the crystal structure of the RPtIn compounds (R = Y, Gd - Lu), room temperature powder X-ray measurements were performed, using Cu K_α radiation. A typical pattern is shown in Fig.1 for TbPtIn. All detected peaks were indexed using the Rietica Rietveld refinement program, with the $P\bar{6}2m$ space group and lattice parameters $a = (7.56 \pm 0.01)$ $\AA$ and $c = (3.87 \pm 0.01)$ $\AA$, and no secondary phases were detected. In Fig.2, the volume and the dimensions of the unit cell across the series are shown as a function of the R^{3+} ionic radii. All values shown in this figure are calculated from high angle/high intensity peaks, *i.e.*, using the (231) and (032) peaks, together with the corresponding error bars which also encompass the values yielded by the Rietica refinement. The unit cell volume (Fig.2a) generally follows the expected lanthanide contraction[18] (as shown by the dotted line), as does the c lattice parameter (Fig.2b), whereas an apparent non-monotonic change of the a parameter is noticeable in Fig.2c. However, the R = Tm and Yb volumes appear to deviate slightly from the monotonic decrease across the series; whereas this could indicate, at least for R = Yb, a trend toward valence 2+ for the rare earth ions, we shall see that the magnetic measurements are consistent with the presence of magnetism in the respective compounds, associated with trivalent R ions.

Additional single crystal x-ray measurements were performed on the R = Tb, Tm and Yb members of the series; these data indicated a small (*i.e.*, less than 6 %) deficient occupancy of one of the two Pt sites in the unit cell of the R = Yb system, leading to a stoichiometry closest to $YbPt_{0.97}In$. The analogous measurements on TbPtIn and TmPtIn crystals indicated full occupancy on all crystallographic sites in these compounds. The lattice parameters from single crystal X-ray data for all three compounds are consistent with the powder values in Fig.2.

Magnetic measurements were performed in a Quantum Design Magnetic Properties Measurement System (MPMS) SQUID magnetometer (T = 1.8 - 350 K, H_{max} = 55 kG). Additional measurements up to 140 kG were also taken for TbPtIn, using an extraction magnetometer in a Quantum Design Physical Properties Measurement System (PPMS). We measured anisotropic field and temperature dependent magnetization for all compounds, having the applied field $H \parallel c$ or $H \parallel ab$, with arbitrary orientation of the field within the basal plane unless otherwise specified. The corresponding susceptibilities were calculated as M / H, whereas the polycrystalline average susceptibility was estimated to be

$$\chi_{ave} = 1/3 * (\chi_c + 2 * \chi_{ab}),$$

or, when in-plane anisotropic measurements were available (*i.e.*, for the external field $H \parallel [100]$ and $H \parallel [120]$),

$$\chi_{ave} = 1/3 * (\chi_{[100]} + \chi_{[120]} + \chi_{[001]}).$$

Curie-Weiss behavior of the anisotropic susceptibilities was observed for all magnetic compounds, such that $\chi = C / (T + \Theta_W)$. Thus from the high-temperature linear inverse susceptibilities we were able to determine both the effective moment μ_{eff} (and compare it with the expected free ion value) and the anisotropic Weiss temperatures Θ_W for each compound.

Additional angular dependent magnetization measurements have been performed on the HoPtIn compound, as well as on the corresponding dilution with non-magnetic Y^{3+} ions on the Ho site, $Ho_xY_{1-x}PtIn$ (x $\simeq$ 0.04). For these measurements, the angular position of the samples was controlled by a specially modified MPMS sample holder which allowed for the rotation of the sample so that either the [001], [100] or [120]-axis stayed perpendicular to the applied magnetic field. Torque on the rotor was avoided by using small mass samples for the rotation measurements, and these data were subsequently calibrated with the two directions M(H) data on larger mass samples, as described in more detail by Morosan *et al.*[14].

Heat capacity measurements were made in the same Quantum Design PPMS system. For each measurement, the sample holder and grease background data, taken separately, were later subtracted from the sample response.

For the antiferromagnetic members of the series (R = Tb and Tm), we inferred the transition temperatures (Néel temperature or spin reorientation temperatures) as determined from $d(M_{ave}/H * T)/dT$[19] and $C_p(T)$ plots. In the ferromagnetic RPtIn compounds, unusually broad peaks marked the ordering in the specific heat data. Thus the onset of the transition was chosen as the Curie temperature T_C (*i.e.*, the T value for which an increase of the specific heat data occurs as the temperature is lowered through the phase transition).

III. RESULTS

We are characterizing each compound by anisotropic magnetization and specific heat measurements, starting with the non-magnetic YPtIn and LuPtIn members of the series. Next the magnetic RPtIn will be introduced, for R = Gd to Tm. For each, we will emphasize the nature of the ordered state together with the ordering temperatures, as well as the high field, anisotropic magnetization data, as these provide key values in our discussion and analysis following the data presentation. Lastly, similar data on YbPtIn is presented, with a note that a more detailed analysis of the heavy fermion character of this compound is the subject of a separate investigation[20].

A. YPtIn and LuPtIn

The anisotropic susceptibilities of the two members of the RPtIn series with non-magnetic R ion (R = Y and Lu) are very small and basically temperature-independent. However, the dominant terms in the susceptibility data seem quite different for the two compounds, as the average high-temperature values are positive in the case of YPtIn (around (6.6 $\pm$ 0.7) $\times$ 10^{-5} emu/mol for $H \parallel ab$, and (4.6 $\pm$ 1.1) $\times$ 10^{-5} emu/mol for $H \parallel c$), and negative for LuPtIn (around ($-$3.8 $\pm$ 0.2) $\times$ 10^{-4} emu/mol for $H \parallel ab$, and ($-$4.5 $\pm$ 0.3) $\times$ 10^{-4} emu/mol for $H \parallel c$). The field-dependent magnetization values for both compounds are extremely small, as expected for non-magnetic R compounds.

Heat capacity measurements in zero applied field were performed for the two systems, for 2 $\leq$ T $\leq$ 90 K. As seen in Fig. 3, they have similar temperature dependencies; the higher molecular weight for LuPtIn (and consequently the expected lower Debye temperature) could explain the values of the specific heat data being larger for this compound than for YPtIn. However, this does not account for the big entropy difference for these two systems (upper inset). This estimated entropy difference has a fairly large value $\Delta S \approx 0.9 * R \ln 2$ around 67 K, which, as we shall see, is the magnetic ordering temperature for GdPtIn. (The entropy difference is still considerably large when the measured specific heat data are scaled by their molecular weights, according to the Debye model.) Consequently, no meaningful magnetic specific heat estimates can be made for the magnetic RPtIn compounds using either the R = Y or Lu compounds as the non-magnetic analogues.

B. RPtIn, R = Gd - Tm

GdPtIn

The anisotropic H / M data for GdPtIn, together with the polycrystalline average, are shown in Fig.4. The inset

presents the low-temperature M / H data for low applied field (H = 100 G), measured on warming up after either zero-field cooling ZFC (symbols) or field cooling FC (solid lines) of the sample. The paramagnetic susceptibility shows Curie-Weiss behavior $\chi(T) = C/(T + \Theta_W)$ above $\sim$ 100 K. Θ_W represents the Weiss temperature, which can be determined from the linear fit of the high-temperature inverse susceptibility, and the values corresponding to the two orientations of the field, as well as the one for the polycrystalline average, are listed in Table 1. The inverse susceptibility data appear slightly anisotropic, contrary to the expected isotropic paramagnetic state for a Gd compound. This is possibly caused by the dominant anisotropic interaction in a pure S-state (*i.e.*, L = 0) compound[21], also consistent with the different anisotropic Weiss temperatures for this Gd system (see Table 1). The effective moment value determined from the linear region in the inverse average susceptibility is $\mu_{eff} = 7.62\ \mu_B$, comparable to the theoretical value of 7.94 μ_B for the Gd^{3+} ions.

The field dependent magnetization data (Fig.5) appears to indicate ferromagnetic ordering along the c-axis. Measurements performed for both increasing and decreasing applied field reveal hysteresis loops for both H parallel and perpendicular to the c-axis. At $H \approx 50$ kG, the magnetization saturates in both directions around the expected 7 μ_B/ Gd^{3+} value. As the increase of the axial magnetization with field (*i.e.*, for $H \parallel c$) is much faster than for $H \perp c$, we are led to believe that the ferromagnetic exchange interaction favors moments' alignment along the c-axis.

There is significant difference between the ZFC and the FC data in the ordered state for both $H \parallel ab$ and $H \parallel c$, with $\chi_c > \chi_{ab}$ in the low-temperature paramagnetic state (inset Fig.4). This is consistent with the magnetic moments ordering ferromagnetically along the c-axis below the irreversibility temperature $T_{irr} = 63.8 \pm 1.9$ K, as it has already been reported on polycrystalline samples by Watson *et al.*[13]. The irreversibility temperature for $H \parallel ab$ is slightly different ($\sim$ 65.2 K). Specific heat data is needed to determine the magnetic ordering temperature, and using an on-set criterion (Fig.6), the Curie temperature was determined to be $T_C = 67.5 \pm 0.5$ K, larger than the anisotropic T_{irr} values. In turn, this value is significantly lower than the previously reported ordering temperature for the polycrystalline samples[13]. We believe that the discrepancies in the ordering temperature estimates are due to the different criteria used for determining T_C, as well as to the different types of samples used in the measurements, with the single crystal data possibly being more accurate.

TbPtIn

We have already looked in detail at the magnetic and transport properties of TbPtIn[14]: in contrast to the neighboring R = Gd member of the series, TbPtIn has an antiferromagnetic ground state below $T_N = 46.0$ K, with an extremely anisotropic, planar susceptibility even in the paramagnetic state (Fig.7). At higher temperatures, the inverse average susceptibility becomes linear, indicating Curie-Weiss like behavior. Extrapolation of the polycrystalline linear fit down to low temperatures yields an effective moment value $\mu_{eff} = 9.74\ \mu_B$, in good agreement with the theoretical value 9.72 μ_B for Tb^{3+} ions. The anisotropic Weiss temperatures were also determined, and the corresponding values are given in Table 1. Another phase transition is apparent around $T_m = 27.4$ K, possibly associated with a spin reorientation. This phase transition was obscured in the measurements on polycrystalline samples[13], whereas the T_N value that we determined based on measurements on single crystals is fairly close to the previously reported one.

As already seen by Morosan *et al.*[14], the TbPtIn specific heat shown in Fig.8a confirms the Néel temperature and the lower temperature transition at T_m (marked by the vertical dotted lines). These transition temperatures are also consistent with those revealed by the $d(M_{ave}/H * T)/dT$ data (Fig.8b), as expected for antiferromagnetic compounds[19].

Anisotropic field-dependent measurements at $T = 2$ K (Fig.9) reveal the presence of several metamagnetic transitions for field applied perpendicular to the hexagonal c-axis, whereas for field along the c-axis an almost linear increase of the magnetization with field is observed up to $\sim$ 140 kG. As emphasized by Morosan *et al.*[14], apart from the extreme in-plane/out-of-plane anisotropy, there is also a complex angular dependence of the observed metamagnetism for $H \perp c$. The full and open circles in Fig.9 represent the measurements corresponding to the two high symmetry in-plane directions of the applied field (*i.e.*, the [120] and [110] directions respectively), for increasing and decreasing fields. The high-field magnetization values reach 6.45 μ_B / Tb^{3+} and 5.86 μ_B/ Tb^{3+} for the two in-plane directions, and, within the *three coplanar Ising-like model*[14], correspond to the crystal field limited saturated paramagnetic CL-SPM state. Also consistent with this model in the low energy limit is the low value of the axial component of the magnetization $M([001]) = 0.92\ \mu_B$ / Tb^{3+}. However, a slow increase of the high-field magnetization plateaus is apparent for $H \perp c$; this, as well as the slow increase of M_c with the applied field, may be due to the fact that the system is approaching the CEF splitting energy scale. Extrapolation of the high-field magnetization data (solid lines in Fig.9) down to $H = 0$ leads to smaller values (*i.e.*, 6.13 μ_B, 5.86 μ_B and 0 for $M([120])$, $M([110])$, and $M([001])$ respectively), even closer to the theoretical ones[14].

DyPtIn

So far we have seen that GdPtIn has a ferromagnetic ground state, with $\chi_c > \chi_{ab}$ in the low-temperature paramagnetic state, whereas TbPtIn orders antiferromagnetically and is extremely planar, even for a limited

temperature range above T_N.

As we move towards the heavier R members of the series, DyPtIn resembles more the R = Gd compound rather than the neighboring R = Tb one: from the anisotropic H / M data data shown in Fig.10, it appears that DyPtIn has a linear inverse average susceptibility, from which an effective moment $\mu_{eff} = 10.7\ \mu_B$ can be determined, consistent with the theoretical value of 10.6 μ_B. The anisotropic inverse susceptibilities can also be used to determine the Weiss temperatures, listed in Table.1 for both orientations of the field, as well as for the polycrystalline average. Below $\sim$ 30 K, DyPtIn orders magnetically (the Curie temperature T_C will be determined from the specific heat data, shown below). The ordered-state M / H data indicates a possible net ferromagnetic component along the c-axis. Moreover, ZFC and FC data for $H = 100$ G (inset, Fig.10) further confirm this hypothesis, given the irreversibility of the χ_c data below $\sim$ 25 K, and no visible irreversibility for the χ_{ab} data.

As previously seen for GdPtIn, a rather broad peak in the specific heat data (Fig.11) indicates the magnetic ordering of the DyPtIn. Using the on-set criterion, the Curie temperature is determined to be $T_C = (26.5 \pm 0.5)$ K, indicated by the small vertical arrow. The substantial difference between our estimates and those of Watson et al.[13] for the ordering temperature, which appears to persist for all RPtIn members (R = Gd - Dy) described so far, could be a consequence of the two sets of data having been collected on single crystal or polycrystalline samples, respectively. However, for the ferromagnetic compounds, different criteria used for determining the ordering temperature may also be causing the aforementioned differences.

The field-dependent magnetization loops ($-$ 55 kG $\leq H \leq$ 55 kG) are shown in Fig.12, for both $H \parallel c$ and $H \perp c$. For the applied field along the c-axis (crosses), a small hysteresis can be observed, whereas the magnetization rapidly increases towards a saturated-like value around $\sim$ 6.88 μ_B / Dy^{3+}. This is consistent with a ferromagnetic component of the magnetization along the c-axis, which is well below the expected 10 μ_B saturated value for Dy^{3+} ions. For $H \perp c$, a metamagnetic transition occurs around $\sim$ 37 kG, leading to a state with the magnetization value around 4.98 μ_B, even smaller than the axial component. As we shall see for the rest of the local-moment members of the series (R = Ho, Er, Tm), the measured values of the magnetization at the highest applied field are far smaller than the theoretical saturated values for the respective ions, for both $H \parallel c$ and $H \perp c$. Starting from the two-dimensional model already developed for TbPtIn[14], we will attempt to generalize it to three dimensions such as to explain the nature of the ordered state across the whole RPtIn series (R = Gd - Tm).

HoPtIn

HoPtIn has similar physical properties to GdPtIn and DyPtIn, and appears to conform to some general characteristics of the RPtIn series, with the Tb member as an apparent exception: axial ferromagnetic component of the ordered state magnetization, less than the theoretical saturated values above $\sim$ 50 kG for both the axial and the planar magnetizations.

As can be seen in Fig.13, the anisotropic inverse susceptibilities are linear at high temperatures; from the polycrystalline average, we get an effective moment of 10.5 μ_B, close to the theoretical value $\mu_{eff}(Ho^{3+}) = 10.6\ \mu_B$. The presence of the ferromagnetic component of the ordered state is evidenced by the anisotropic M / H data featuring a large, broad peak at low temperatures for $H \parallel c$ (inset Fig.13), with $\chi_c > \chi_{ab}$ in the low-temperature paramagnetic state. In the specific heat data (Fig.14), magnetic ordering is apparent below $T_C = 23.5 \pm 0.5$ K, as indicated by the small arrow.

The idea of a ferromagnetic component of the magnetization is further confirmed by the field dependent data in Fig.15, where for the field applied in the c direction (crosses), the magnetization rapidly increases with H. The maximum value reached within our field limits is $\sim$ 7.81 μ_B, less than the calculated saturated moment for Ho^{3+} ions. As the magnetic field is applied parallel to the basal plane, the resulting magnetization curve is consistent with either a broad metamagnetic transition or with a continuous spin-flop transition. Around $H = 55$ kG, the in-plane component of the magnetization is 4.3 μ_B, even smaller than the axial one and less than half of $\mu_{sat}(Ho^{3+})$.

ErPtIn

As TbPtIn appears to be an exception, the R = Er member of the RPtIn series follows the already observed trends for the other heavy R compounds. The H / M average data seen in Fig.16 is linear towards high temperatures, indicative of Curie-Weiss behavior of magnetization. However, crossing of the planar and axial inverse susceptibilities occurs around 150 K, possibly a result of strong crystal field effects at high temperatures in this compound. Similar crossing of the anisotropic inverse susceptibilities was also observed for the R = Er member of the RNi_2B_2C series[22]. The effective moment value extracted from the high-T linear region of the inverse average susceptibility is $\mu_{eff} = 10.1\ \mu_B$, close the theoretical 9.6 μ_B value (within the accuracy of our data and fit).

The low temperature anisotropic H / M data shown in the inset is consistent with ferromagnetic ground state, with $\chi_c > \chi_{ab}$ in the low-T paramagnetic state. The Curie temperature, as determined from the specific heat data in Fig.17, is $T_C = 8.5 \pm 0.5$ K, as the small arrow indicates.

From the field-dependent measurements in Fig.18 we also infer that the magnetization has a ferromagnetic component along the c-axis, as the corresponding data

(crosses) rapidly increase with field. Above $\sim$ 10 kG, the axial magnetization has an almost constant value around 7.50 μ_B, whereas the theoretical saturated moment for Er^{3+} ions is 9 μ_B. When $H \perp c$ (open circles), the magnetization data is almost linear in field, with a weak hint of un upward curvature around 20 kG, possibly indicating a metamagnetic transition. Towards 50 kG, the magnetization almost levels off around a 2.77 μ_B value, much lower than the expected saturated moment.

TmPtIn

Having an antiferromagnetic ground state and a planar magnetization component larger than the axial one, TbPtIn differs from the rest of the RPtIn compounds mentioned so far, whereas below we show that it resembles the R = Tm member of this series.

The high temperature inverse susceptibility of TmPtIn (Fig.19) is linear, yielding an effective magnetic moment around 7.7 μ_B, close to the theoretical value calculated for Tm^{3+} ions, $\mu_{eff} = 7.6\ \mu_B$. However, unlike the aforementioned members of the series (except Tb), below $\sim$ 4 K this compound appears to order antiferromagnetically, as suggested by the low-temperature susceptibility data in the inset. Sharp peaks in the susceptibility data around T_N are typically indicative of antiferromagnetic ordered state, as is the case with the $H \parallel c$ data (crosses) shown in the inset in Fig.19. The similar peak for the in-plane susceptibility (open circles) is somewhat broader, possibly due to spin fluctuations or CEF effects, which result in reduced susceptibility values around the ordering temperature.

A peak in the specific heat (Fig.20a) suggests that the magnetic order occurs at $T_N = 3.0 \pm 0.5$ K, and, as expected for antiferromagnetic compounds[19], is consistent with the $d(M_{ave}/H * T)/dT$ data in Fig.20b.

The $T = 2$ K magnetization isotherms (Fig.21) indicate one (for $H \parallel c$) or more (for $H \parallel ab$) metamagnetic transitions. Following these fairly broad transitions (due to the high temperature, compared to T_N, for which these data were taken), the magnetization curves seem to approach some horizontal plateaus around 2.26 μ_B for the field along the c-axis, and 4.42 μ_B for the field within the ab-plane respectively. As for the other RPtIn (except for R = Gd), both these values are much smaller than the calculated effective moment of 7 μ_B for the Tm^{3+} ions.

C. YbPtIn

YbPtIn stands out from the rest of the RPtIn compounds through a number of distinctly different properties. Fig.22 shows the inverse anisotropic susceptibilities (symbols), together with the calculated polycrystalline average (solid line). The latter data is linear above $\sim$ 50 K, despite a pronounced departure from linearity of the axial inverse H / M data (crosses) below $\sim$ 200 K, probably due to CEF effects. From the fit of the linear part of the average H / M data, an effective moment of 4.3 μ_B/ Yb^{3+} can be determined, close to the theoretical 4.5 μ_B/ value. For lower temperatures, no distinguishable features associated with magnetic order are visible in the M / H data data down to 1.8 K (inset, Fig.22), for field values of 0.1 and 20 kG. This observations are consistent with the susceptibility data reported by Kaczorowski *et al.*[11]. However, the specific heat data (Fig.23) shows a sharp peak around 2.1 K, and the feature associated with this transition could have been missed in the M / H measurements because of the limited temperature range below the transition.

Trovarelli *et al.*[10] presented magnetization measurements that, for low applied fields ($H = 0.1$ kG), suggest antiferromagnetic ordering below $T_N = 3.4$ K, a value that is different from the possible transition temperature indicated by our measurements. In trying to understand the possible cause of such differences, single crystal x-ray measurements were performed. They indicate that our flux-grown YbPtIn single crystals have a partial (*i.e.*, $\sim$ 94 %) occupancy for one of the two Pt sites in the unit cell, such that the stoichiometry of these crystals is closest to $YbPt_{0.97}In$. This is not entirely surprising, given the different flux growth process (a low Pt-concentration used in the initial $Yb_{0.4}Pt_{0.1}In_{0.5}$ solution). Consequently the R = Yb compound is excluded from the following discussion. A more complete analysis of the thermodynamic and transport properties of this material is currently the subject of a different study[20].

IV. DATA ANALYSIS

The magnetic RPtIn compounds that we investigate here appear to order magnetically below $\sim$ 70 K. As can be seen in Fig.24, their ordering temperatures T_{ord} scale fairly well with the de Gennes factor $dG = (g_J - 1)^2\ J\ (J + 1)$, where g_J is the Landé g-factor, and J is the total angular momentum of the R^{3+} ion Hund's rule ground state. Whereas this suggests that the RKKY interaction between the conduction electrons and the local magnetic moments gives rise to the long-range magnetic order, slight departures from linearity, similar to those seen for other rare earth-series[23,24,25], are due to the extremely simplified assumptions associated with the de Gennes scaling. The scaling is apparently unaffected by the curious switching from ferromagnetic to antiferromagnetic ordering across the RPtIn series, which appears to be correlated with a change in the anisotropy, such that, in the low-T paramagnetic state, $\chi_c > \chi_{ab}$ for the ferromagnetic compounds, and $\chi_{ab} > \chi_c$ for the antiferromagnetic ones. At first, this may seem inconsistent with de Gennes scaling, which would indicate similar ordering mechanisms for all RPtIn compounds, R = Gd - Tm. As we shall see, we believe that, because of their

Fe_2P-type hexagonal structure, with three R ions sitting at orthorhombic point symmetry sites, strong CEF effects constrain the local magnetic moments in R = Tb - Tm to equivalent non-collinear easy-axes. This results in (i) anisotropic paramagnetic magnetization, and (ii) crystal field limited saturated paramagnetic CL-SPM states with magnetization values well below the corresponding free ion saturated moments.

We have already modelled the effects of strong crystal electric fields on the Fe_2P-type crystal structure, for the case of the extremely planar R = Tb member of the RPtIn series and the similar R = Tm member of the RAgGe series, using the *three co-planar Ising-like systems model*[14]: having three rare earths in orthorhombic point symmetry, the hexagonal symmetry of the unit cell was achieved by constraining the local moments to three equivalent co-planar directions, 60^0 away from each other. In allowing both the "up" and "down" positions (*i.e.*, Ising-like) for each of the three magnetic moments, the antiferromagnetic ground state was, in the simplest case, realized by a ($\searrow\uparrow\swarrow$) moment configuration (Fig.25a); upon increasing the applied magnetic field within the basal plane, a number of metamagnetic states occurred, showing simple dependencies of the critical fields H_c and the locally saturated magnetizations M_{sat} on the angle θ between the direction of the field and the easy axis (see Fig.13 and related discussion by Morosan *et al.*[14]). When all the moments are in their "up" positions ($\nwarrow\uparrow\nearrow$), a crystal field limited saturated paramagnetic CL-SPM state is reached (Fig.25b); the expected magnetization value is

$1/3 * \mu_{sat}(Tb^{3+}) * (1 + 2 * \cos 60^0) = 2/3 * \mu_{sat}(Tb^{3+})$ or $2/3 * 9\ \mu_B = 6\ \mu_B$,

consistent with the easy-axis measured data (full circles) shown in Fig.9.

We thus see that the aforementioned *three co-planar Ising-like systems model* explains how the measured magnetization values can be much smaller than the theoretical saturated value of 9 μ_B for the Tb^{3+} ions.

By contrast, the GdPtIn doesn't exhibit such reduced values of the magnetization for high applied fields (Fig.5), given that the Gd^{3+} ions are in a symmetric $^8S_{7/2}$ state, and thus the CEF effects are minimal: for $H \parallel c$ (crosses), the magnetization rapidly increases, reaching $\mu_{sat}(Gd^{3+}) = 7\ \mu_B$ for $H \geq 10$ kG. This is typical of a ferromagnetic magnetization for field applied along the direction of the moments (easy axis). Furthermore, the $H \perp c$ data (open circles) represent classical hard axis data, and are consistent with axial ferromagnetic ordering in this compound, as the saturated state is also reached, however at a slower rate (*i.e.*, for $H \geq 40$ kG).

For the other neighboring TbPtIn compound, the DyPtIn magnetization resembles the similar data for GdPtIn, even though the presence of CEF effects in the former system results in reduced magnetization values at our maximum applied field: as can be seen in Fig.12, the $H \parallel c$ magnetization (crosses) rapidly increases with field, as expected for a ferromagnet with moments along c, but at $H = 55$ kG its value is only ~ 0.7 of the theoretical saturated moment of 10 μ_B. For field applied within the basal plane (open circles), only 0.5 of the saturated moment is reached following a metamagnetic transition around 35 kG. Whereas more metamagnetic transitions beyond our maximum field of 55 kG could account for the small magnetization values in this compound, such a hypothesis does not address one more peculiarity already apparent for the RPtIn series: even though the R = Gd and Dy compounds are ferromagnetic, and the R = Tb one is antiferromagnetic, their ordering temperatures scale well with the de Gennes factor, as we showed in Fig.24. Furthermore, the R = Ho and Er compounds also display ferromagnetic components of the ordered state magnetization, whereas TmPtIn is antiferromagnetic, and yet the de Gennes scaling still holds for all heavy RPtIn compounds (Fig.24). The question arises whether a generalized hypothesis exists, which could account for the magnetic ordering in all RPtIn systems (R = Gd - Tm), or whether TbPtIn and TmPtIn should be regarded as exceptions from the ferromagnetic axial ordering across the series.

In what follows we will present one plausible model for the magnetic ordering in the local moment RPtIn compounds, a generalized version of the two-dimensional *three Ising-like systems model*, which addresses the above points. We first proposed such a model for DyAgGe[25], an isostructural compound to RPtIn, for which a ferromagnetic component of the magnetization was also apparent along the c-axis.

In the *three co-planar Ising-like systems model*, we assume that the magnetic moments are allowed to three orientations (along any three of the six equivalent six-fold symmetry axes within the basal plane), with two positions ("up" and "down") per orientation. This results in a set of three two-fold degenerate easy-axes, 60^0 away from each other, the degeneracy being a direct consequence of the requirement that the Ising-like systems be co-planar: the "up" position for a given easy-axis is indistinguishable from the "down" position for the equivalent direction $3 * 60^0 = 180^0$ away.

If we release the restriction that the moments be co-planar, while still imposing that their *in-plane* projections be 60^0 away from each other to preserve the hexagonal symmetry of the crystals, this degeneracy is lifted, and the moments are not necessarily Ising-like systems any more. The three-dimensional model described above can be directly derived from the planar one, as follows: we consider that Fig.25 represents the *in-plane* projection of the magnetic moments' configuration, to which non-zero axial components of the moments are added. The possible resulting moment configurations can be obtained using any combination of "up" (thin solid arrows) or "down" (thin dotted arrows) planar and axial components of the magnetic moments, as shown in Fig.26. Given the orthorhombic point symmetry of the magnetic moments' sites, this yields two possible co-planar orientations for each magnetic moment, with the correspond-

ing "up" and "down" positions for each. The thick solid arrows in Fig.26 represent the full magnetic moments, which are parallel to three non-planar, equivalent directions (*i.e.*, easy axes), inclined at an angle α from the c-axis. This configuration corresponds to the crystal field limited saturated paramagnetic CL-SPM state, where all *in-plane* and axial components of the magnetic moments are in their respective "up" positions.

It is worth noting that, by analogy with the two-dimensional model, there are two sets of easy axes: the [1 2 l]-equivalent axes, where l is the c-axis Miller index, for which the corresponding *in-plane* model exactly describes TbPtIn, or the [1 1 l]-equivalent directions, with a two-dimensional analogous example being TmAgGe (also described in detail by Morosan *et al.*[14]). In our present model and data analysis, we are assuming the first scenario, in which the easy axes are the [1 2 l]-equivalent directions, which project in the ab-plane onto the [1 2 0] directions. Consequently we will refer to the (1 2 0) planes as the "easy" planes and the [1 2 0] directions as "easy" *in-plane* axes, whereas the (1 1 0) planes and the [1 1 0]-axes will be called in this case "hard" planes and "hard" *in-plane* axes respectively. When the [1 1 l] directions are the easy axes, the same description is still valid, with the "easy" and "hard" planes and *in-plane* directions interchanged from the previous case.

We have thus introduced a model generalized from the *three co-planar Ising-like systems model*, which takes into account the CEF effects on hexagonal compounds with orthorhombic point symmetry of the rare earths. For each compound, the strength of the CEF effects will be reflected by the value of the angle α between the easy-axes and the c-axis. At low temperatures, another energy scale is introduced by the applied magnetic field, and the model described above is only valid for fields much smaller than the CEF energy. In this limit, for the highest applied fields, a CL-SPM state is reached, for which the anisotropic magnetization values are smaller than the theoretical saturated moments μ_{sat} for the respective R ions.

For a fixed angle α, there are six possible easy-axes (or three pairs of co-planar easy axes), each with the corresponding "up" and "down" positions. As in the case of the two-dimensional model, multiples S of three moments may be required to characterize the moment configuration for a given applied field. The orientation of the applied field will determine the magnetic moments to align along the three easy axes closest to the direction of the field, whereas its magnitude will determine the number of "up" and "down" moments along those three easy axes.

The CL-SPM state is reached when all three magnetic moments are in their "up" positions along three adjacent easy axes closest to the field direction (or, equivalently, when all *in-plane* and axial components of the magnetic moments are in their "up" positions). This state is illustrated in Fig.26, for the magnetic field applied off the c-axis. (If H is parallel to the c-axis, all six "up" positions of the magnetic moments are equally probable, and only when rotating the field away from c the three easy axes closest to the applied field direction are uniquely determined).

Experimentally we can only measure the projection of the magnetic moments along the field direction, with the resulting magnetization per magnetic moment given by $M = \frac{1}{3}\,[\,\overrightarrow{M}_1 + \overrightarrow{M}_2 + \overrightarrow{M}_3\,] \cdot \frac{\overrightarrow{H}}{H}$.

Moreover, we were able to measure the angular dependent magnetization for the magnetic field applied within the horizontal ab-plane and the high-symmetry vertical planes (*i.e.*, "easy" or "hard" planes). Such data can be used to probe the validity of our model, by comparison with the theoretical calculation of the expected angular dependent "easy" and "hard" magnetization values.

For a fixed angle α, and for field making an angle θ with the c-axis, the magnetization values $M^e(\theta)$ and $M^h(\theta)$ in the CL-SPM state are, as calculated in detail in the Appendix:

$$M^e_{CL-SPM}/\mu_{sat}(\mathrm{R}^{3+}) = \frac{2}{3} * \sin\alpha * \sin\theta + \cos\alpha * \cos\theta$$

and

$$M^h_{CL-SPM}/\mu_{sat}(\mathrm{R}^{3+}) = \frac{\sqrt{3}}{3} * \sin\alpha * \sin\theta + \cos\alpha * \cos\theta,$$

where θ is the angle between the applied magnetic field and the c-axis, and the indexes "e" and "h" denote, respectively, the "easy"- and "hard"-plane components of the magnetization. As already mentioned, we assume the "easy" and "hard" axes to be the [1 2 0] and the [1 1 0] directions, respectively. In what follows, our analysis refers only to the CL-SPM state, therefore the subscript denoting the respective state has been dropped for clarity.

From these calculations, the expected magnetization components (in units of $\mu_{sat}(\mathrm{R}^{3+})$) for field parallel or perpendicular to the c-axis are:

$M([001]) = M^e(\theta = 0^0) = M^h(\theta = 0^0) = \cos\alpha \leq 1,$

$M([120]) = M^e(\theta = 90^0) = \frac{2}{3}\sin\alpha < 1$

and

$M([110]) = M^h(\theta = 90^0) = \frac{\sqrt{3}}{3}\sin\alpha < 1.$

Moreover, local maxima for the M^e and M^h curves are reached for $\theta_{max} = \arctan(\frac{2}{3}\tan\alpha)$, and $\arctan(\frac{\sqrt{3}}{3}\tan\alpha)$ respectively, with the corresponding magnetization values equal to $\sqrt{\cos^2\alpha + (\frac{2}{3})^2\sin^2\alpha} = \sqrt{1 - \frac{5}{9}\sin^2\alpha} < 1,$ and $\sqrt{\cos^2\alpha + (\frac{\sqrt{3}}{3})^2\sin^2\alpha} = \sqrt{1 - \frac{6}{9}\sin^2\alpha} < 1.$

As can be seen from the above calculations, one should expect the measured magnetization values to be smaller than the theoretical saturated moment $\mu_{sat}(\mathrm{R}^{3+})$, regardless of the direction of the applied field. The only exception is the axial magnetization $M([001])$ for $\alpha = 0^0$ (moments parallel to the c-axis), when the expected value is exactly $\mu_{sat}(\mathrm{R}^{3+})$. These observations lend support to the idea that the three-dimensional model considered above could describe the RPtIn compounds, since for all R = Tb - Tm we have indeed observed reduced values of the high-field anisotropic magnetizations. On the other

hand, it appears that the fully saturated magnetization measured for GdPtIn could be described by the above model for $\alpha = 0^0$, but the absence of CEF effects restricts the applicability of our model to this compound.

In the case of TbPtIn the magnetization measurements revealed extreme planar anisotropy of this compound (Fig.7 and 9). Within our three-dimensional model, this is consistent with the angle α being equal to 90^0, when the magnetic moments become co-planar. In this case, the calculated magnetization values become (in units of $\mu_{sat}(\mathrm{Tb}^{3+})$)

$M([001]) = \cos 90^0 = 0$,

$M([120]) = \frac{2}{3} \sin 90^0 = \frac{2}{3}$

and

$M([110]) = \frac{\sqrt{3}}{3} \sin 90^0 = \frac{\sqrt{3}}{3}$.

These values show that when $\alpha = 90^0$, our model indeed reduces to the *three co-planar Ising-like systems model*[14].

When $0^0 \leq \alpha < 90^0$, our model yields axial magnetization values larger than 0, and this is observed for all RPtIn, R = Tb - Tm. Therefore we can verify the applicability of our model to these systems by estimating the angle α, and comparing the measured and calculated magnetization values in the CL-SPM state as follows:

For all RPtIn compounds, the in-plane magnetization measurements were performed for field along the [1 2 0] direction. Since it is not readily apparent whether this represents the "easy" or "hard" in-plane direction, one way to estimate the angle α is from the $M([0\ 0\ 1])$ data:

$M([0\ 0\ 1]) \ / \ \mu_{sat}(\mathrm{R}^{3+}) = \cos\alpha$.

Therefore $\alpha = \arccos(M([0\ 0\ 1]) \ / \mu_{sat}(\mathrm{R}^{3+}))$. These values are listed in Table 2, together with the measured magnetization values M([0 0 1] at $H = 55$ kG, which were used in the above formula. For this value of the angle α, the "easy" and "hard" in-plane magnetization components should be, as described above,

$M^e \ / \ \mu_{sat}(\mathrm{R}^{3+}) = \frac{2}{3} \sin\alpha$

and

$M^h \ / \ \mu_{sat}(\mathrm{R}^{3+}) = \frac{\sqrt{3}}{3} \sin\alpha$.

However, slight misalignments of the samples can occur for $H \parallel c$, which may result in significant errors in our determination of angle α. In order to minimize these errors, another way to determine α is from the ratio of the two anisotropic measured magnetizations:

$M([1\ 2\ 0]) \ / \ M([0\ 0\ 1]) = 2/3 * \sin\alpha \ / \ \cos\alpha$ if the [1 2 0] direction is the easy axis,

or $M([1\ 2\ 0]) \ / \ M([0\ 0\ 1]) = \sqrt{3}/3 * \sin\alpha \ / \ \cos\alpha$ if the [1 2 0] direction is the hard axis. The measured M([1 2 0]) values which were used for these calculations are listed in Table 2.

Thus the angle α is either

arctan (3 / 2 $*$ $M([1\ 2\ 0]) \ / \ M([0\ 0\ 1])$)

or arctan (3 / $\sqrt{3}$ $*$ $M([1\ 2\ 0]) \ / \ M([0\ 0\ 1])$),

and these estimated values are also listed in Table 2 as α^e and α^h.

As can be observed from the angle values listed in Table 2, together with the error bars resulting from the two different calculations, the angle α ranges from 89^0 for TbPtIn, to $\sim 32^0$ for ErPtIn. Our three-dimensional model seems to be consistent with the experimental data for all RPtIn, R = Tb - Tm.

In order to further explore the validity of the above model, angular dependent magnetization measurements were performed for a $\mathrm{Ho}_x\mathrm{Y}_{1-x}\mathrm{PtIn}$ system ($x \approx 0.04$), for the applied field continuously rotated within the (0 0 1) or the (1 2 0) plane. The above R = Ho system was preferred because the $M(H)$ curves in Fig.15 are consistent with CL-SPM saturated state at $H = 55$ kG for both $H \parallel c$ and $H \perp c$, whereas the system with low concentration of magnetic ions was chosen for this measurement in order to check the validity of our model in the single-ion limit. Moreover, the anisotropic field dependent data for the diluted sample (lines, Fig.15) show almost horizontal plateaus for fields higher than $\sim$ 30 kG, with magnetization values close to the corresponding ones for the pure HoPtIn (symbols). The angle α for $\mathrm{Ho}_x\mathrm{Y}_{1-x}\mathrm{PtIn}$, calculated using $M([0\ 0\ 1])\ |_{55\ kG} = 7.41\ \mu_B/$ Ho, is 42.1^0, close to the corresponding value for the pure compound.

The magnetization measured for field applied within the basal plane (*i.e.,* the (0 0 1) plane) reveals the six-fold anisotropic data, with the ratio $M([1\ 1\ 0])$ / $M([1\ 2\ 0])$ close to $cos\ 30^0 \simeq 0.9$, as expected based on the proposed model. The angular dependent magnetization at $H = 55$ kG is shown in Fig.27 (full circles) for $H \parallel (1\ 2\ 0)$. Also shown as solid lines are the calculated $M^e(\theta)$ and $M^h(\theta)$, for fixed $\alpha = 42.1^0$ determined above. As can be seen, the measured data qualitatively reproduces the features expected based on the above model (*i.e.*, two-fold symmetry with respect to both the *c*-axis and the *ab*-plane, local minima corresponding to $H \parallel [001]$ or $\theta = n * 180^0$, n-integer, and maxima at some intermediate angle). More detailed models which would characterize the RPtIn may exist, and determining all of them is beyond the scope of this paper. However, if we restrict our discussion to the three-dimensional model described before, we see that significant departures from both calculated $M^e(\theta)$ and $M^h(\theta)$ curves can still be observed, despite the apparent qualitative agreement between calculations and measured data. This may mean that either a totaly different model needs to be considered, or that the aforementioned model needs further refinement in order to describe at least the HoPtIn, and perhaps the rest of the RPtIn compounds. Furthermore, additional experiments (*i.e.*, neutron diffraction) are required to help identify the most appropriate model for the magnetization of the RPtIn compounds.

V. CONCLUSIONS

Single crystals of the RPtIn compounds (R = Gd - Lu) have been grown using the self-flux technique, and have been characterized by anisotropic temperature- and field-dependent magnetization and zero-field specific heat measurements. A small Pt-deficiency in the YbPtIn is

apparent from single crystal X-ray data, whereas all the other heavy R members of the series are believed to form stoichiometrically. Because of this difference in composition, we leave the characterization of the YbPtIn system to a separate study[20], currently underway.

The magnetic RPtIn compounds order magnetically above 2 K, with the ordering temperatures scaling well with the deGennes dG factor (Fig.24). This is consistent with the coupling between the conduction electrons and the local magnetic moments giving rise to the long-range magnetic order via RKKY exchange interaction. However, the R = Tb and Tm members of the series have antiferromagnetic ground states, whereas in the ordered state, the magnetization of all the other compounds has at least a ferromagnetic component along the c-axis. These discontinuous changes from antiferromagnetic to ferromagnetic state across the series seems to also be associated with a change of low-temperature anisotropy of the paramagnetic state, such that $\chi_{ab} > \chi_c$ for TbPtIn and TmPtIn, and $\chi_{ab} < \chi_c$ for the rest of the magnetic RPtIn.

The magnetization of the TbPtIn compound is extremely anisotropic, with the magnetic moments confined to the ab-plane. Below the antiferromagnetic ordering temperature $T_N = 46.0$ K, a second magnetic phase transition is apparent around 27 K. At low temperature, in-plane magnetization data reveals complex metamagnetism, and this has been studied in detail, and described using the *three co-planar Ising-like systems model* by Morosan *et al.*[14].

Having understood the complex angular dependent metamagnetism in the planar TbPtIn compound, we attempted to generalize the *three co-planar Ising-like systems model* to three dimensions, such as to characterize the magnetically ordered state in the other RPtIn compounds: instead of assuming the moments to be confined to equivalent co-planar directions, 60^0 away from each other, they could be restricted to equivalent directions within vertical planes rotated by 60^0 around the c-axis. This is equivalent with sets of six non-planar easy axes, each at an angle α from the c-axis, with "up" and "down" orientations for each directions. When the applied field is oriented at a non-zero angle from the c-axis, the three magnetic moments will align along the three easy axes closest to the direction of the field. (This implies that at high enough fields, all three moments will be in the "up" positions of three adjacent easy axes, corresponding to the CL-SPM moment configuration.)

The angle α between the easy axes and the c direction is dependent, in each compound, on the crystalline electric field CEF energy. Simple geometrical relations allow us to calculated the expected components of the CL-SPM magnetization along the c-axis, as well as for the "easy" and "hard" in-plane orientations of the field. Assuming that for $H = 55$ kG (in most cases the maximum available field for our measurements), the RPtIn systems indeed reach the CL-SPM state at low temperatures, we can determine the fixed value for the angle α for each compound, and compare the high-field measured magnetization values with the calculated ones.

As can be seen from Table 2, all RPtIn (R = Tb - Tm) are well described by this model, with α values between 89^0 for R = Tb, and $\sim 32^0$ for R = Er. However, such a model does not fully account for the angular dependence of the magnetization, at least in the case of $Ho_xY_{1-x}PtIn$: this is qualitatively reproduced by the model calculations, with considerable differences between the measured and theoretical magnetization values for the whole angular range. Whereas reasonable misorientation of the rotation sample cannot account for these differences, we are led to believe that it is necessary to refine the over-simplified model described here, and also that additional measurements may help clarify the magnetic structure in these RPtIn compounds.

VI. APPENDIX

In a cartesian coordinate system as shown in Fig.26, the three magnetization vectors in the CL-SPM state can be written as

$\overrightarrow{M}_1 = \mu_{sat}(\mathrm{R}^{3+})\ (0,\ \sin\alpha,\ \cos\alpha)$,

$\overrightarrow{M}_2 = \mu_{sat}(\mathrm{R}^{3+})\ (\sin\alpha * \cos 30^0, \sin\alpha * \sin 30^0, \cos\alpha)$

and

$\overrightarrow{M}_3 = \mu_{sat}(\mathrm{R}^{3+})\ (\sin\alpha * \cos 30^0, -\sin\alpha * \sin 30^0, \cos\alpha)$,

whereas, in general, the applied field vector can be written as

$\overrightarrow{H} = (H_x,\ H_y,\ H_z)$.

Thus the general expression for the CL-SPM magnetization M becomes

$M = \frac{1}{3}\ [(0 + \sin\alpha * \cos 30^0 + \sin\alpha * \cos 30^0) * \frac{H_x}{H} + (\sin\alpha + \sin\alpha * \sin 30^0 - \sin\alpha * \sin 30^0) * \frac{H_y}{H} + (\cos\alpha + \cos\alpha + \cos\alpha) * \frac{H_z}{H}]$

or

$M = \frac{\sqrt{3}}{3}\ \sin\alpha\ * \frac{H_x}{H} + \frac{1}{3}\ \sin\alpha * \frac{H_y}{H} + \cos\alpha * \frac{H_z}{H}$.

Experimentally, we are able to measure the angular dependence of the magnetization within the "easy" and "hard" planes. If the magnetic field is continuously rotated within the "easy" plane ((2 1 0) in Fig.26) than, in cartesian coordinates, the vector $\overrightarrow{H}$ becomes

$\overrightarrow{H} = H\ (\cos 30^0 * \sin\theta,\ \sin 30^0 * \sin\theta,\ \cos\theta)$,

where θ is a continuous variable representing the angle between the applied field and the c-axis.

In this case, the angular dependent magnetization becomes

$M^e/\mu_{sat}(\mathrm{R}^{3+}) = \frac{\sqrt{3}}{3}\ \sin\alpha * \frac{\sqrt{3}}{2}\ \sin\theta$

$+\frac{1}{3}\ \sin\alpha * \frac{1}{2}\ \sin\theta + \cos\alpha * \cos\theta =$

$\frac{2}{3} * \sin\alpha * \sin\theta + \cos\alpha * \cos\theta$,

where the index "e" refers to the "easy" plane component.

Similarly, if the magnetic field is rotated within the "hard" (1 1 0) plane, the vector $\overrightarrow{H}$ can be written as

$\overrightarrow{H} = H\ (\cos 60^0 * \sin\theta,\ \sin 60^0 * \sin\theta,\ \cos\theta))$

and the corresponding angular dependent magnetization is

$M^h/\mu_{sat}(\mathrm{R}^{3+}) = \frac{\sqrt{3}}{3} \sin\alpha * \frac{1}{2} \sin\theta$
$+\frac{1}{3} \sin\alpha * \frac{\sqrt{3}}{2} \sin\theta + \cos\alpha * \cos\theta =$
$\frac{\sqrt{3}}{3} * \sin\alpha * \sin\theta + \cos\alpha * \cos\theta.$

The index "h" is used to indicate the "hard" plane component of this magnetization.

Both calculated $M^e(\theta)$ and $M^h(\theta)$ are shown in Fig.27 (solid lines) for fixed $\alpha = 42.1^0$, as calculated for the $Ho_xY_{1-x}PtIn$ system (see text). As expected, the two-fold symmetry with respect to the c-axis ($\theta = 2n * 90^0$, n-integer) and the ab-plane ($\theta = (2n+1) * 90^0$, n-integer) is revealed by both the calculated angular dependent magnetizations.

VII. ACKNOWLEDGMENTS

We are thankful to H. B. Rhee, J. D. Strand and S. A. Law for growing some of the compounds, to Y.A. Mozharivskyj for the single crystal x-ray measurements, and also to Prof. B. Harmon for helpful discussions. Ames Laboratory is operated for the U.S. Department of Energy by Iowa State University under Contract No. W-7405-Eng.-82. This work was supported by the Director for Energy Research, Office of Basic Energy Sciences.

[1] R. Ferro, R. Marazza, G. Rambaldi, Z. Anorg. Allg. Chem. **410** (1974) 219.
[2] V. I. Zaremba, Y. V. Galadzhun, B. D. Belan, A. Pikul, J. Stepien-Damm, D. Kaczorowski, J. Alloys Comp. **316** (2001), 64.
[3] Y. V. Galadzhun, V. I. Zaremba, H. Piotrowski, P. Mayer, H. D. Hoffmann, R. Pöttgen, Z. Naturforsch. B **55** (2000), 1025.
[4] R. Pöttgen, Z. Krist. **211** (1996), 884.
[5] R. Müllmann, B. D. Mosel, H. Eckert, G. Kotzyba, R. Pöttgen, J. Solid State Chem **137** (1998), 174.
[6] T. Fujita, K. Satoh, Y. Maeno, Y. Uwatoko, H. Fujii, J. Magn. Magn. Matter. **76-77** (1988), 133.
[7] M. Kurisu, T. Takabatake, H. Fujii, J. Magn. Magn. Matter. **90-91** (1999), 469.
[8] Y. Yamaguchi, J. Sakurai, F. Teshima, H. Kawanaka, T. Takabatake, H. Fujii, J. Phys: Cond. Mat., **2** (1990), 5715.
[9] K. Satoh, T. Fujita, Y. Maeno, Y. Uwatoko, H. Fujii, J. Phys. Soc. Japan, **59** (1990), 692.
[10] O. Trovarelli, C. Geibel, R. Cardoso, S. Mederle, R. Borth, B. Buschinger, F. M. Grosche, Y. Grin, G. Sparn, F. Steglich, PRB **61** (2000), 9467.
[11] D. Kaczorowski, B. Andraka, R. Pietri, T. Cichorek, V. I. Zaremba, PRB **61** (2000), 15255.
[12] S. Yoshii, K. Kindo, K. Katoh, Y. Niide, A. Ochiai, J. Magn. Magn. Matter. **272-276** (2004), e99.
[13] K.C. Watson, J. Crangle, K.-U. Neumann and K.R.A. Ziebeck, J. Magn. Magn. Matter. **140-144** (1995), 883.
[14] E. Morosan, S. L. Bud'ko, P. C. Canfield, Phys. Rev. B (accepted for publication, September 2004).
[15] Z.Fisk and J.P.Remeika, *Handbook of the Physics and Chemistry of Rare Earths*, Vol.12 (1989), 53.
[16] P.C.Canfield and Z.Fisk, Phil.Mag. B **65** (1992), 1117.
[17] P.C.Canfield and I.R.Fisher, J. Cryst. Growth **225** (2001), 155.
[18] R. D. Shannon, Acta Cryst. A **32** (1976), 751.
[19] M.E.Fisher, Phil. Mag. **7** (1962), 1731.
[20] E. Morosan, S.L.Bud'ko, Y.A. Mozharivskyj and P.C.Canfield (unpublished).
[21] J. Jensen and A. R. Mackintosh, *Rare Earth Magnetism* (Oxford University Pres, Oxford)
[22] B.K.Cho, P.C.Canfield, L.L.Miller and D.C.Johnston, Phys. Rev. B, **52** (1995) 3684.
[23] K.D.Myers, S.L.Bud'ko, I.R.Fisher, Z.Islam, H.Kleinke, A.H.Lacerda and P.C.Canfield, J. Magn. Magn. Mater., **205** (1999) 27.
[24] S.L.Bud'ko, Z.Islam, T.A.Wiener, I.R.Fisher, A.H.Lacerda and P.C.Canfield, J. Magn. Magn. Mater., **205** (1999) 53.
[25] E. Morosan, S.L.Bud'ko, P.C.Canfield, M. S. Torikachvili and A.H.Lacerda, J. Magn. Magn. Mater., **277** (2004) 298.

TABLE I: Magnetic ordering temperatures, T_m, effective magnetic moments and anisotropic paramagnetic Weiss temperatures Θ_W.

	Gd	Tb	Dy	Ho	Er	Tm	Yb
T_m(K)	67.5 ± 0.5	46.0 ± 0.5 27.4 ± 0.5	26.5 ± 0.5	23.5 ± 0.5	8.5 ± 0.5	3.0 ± 0.5	2.1 ± 0.2
$\mu_{eff}(\mu_B)$	7.6	9.7	10.7	10.5	10.1	7.7	4.3
Θ_{ab}(K)	− 57.2 ± 1.5	− 38.1 ± 1.4	− 2.2 ± 5.2	7.5 ± 0.2	14.5 ± 10.8	− 7.8 ± 2.2	8.2 ± 0.9
Θ_c(K)	− 67.9 ± 0.5	− 29.2 ± 3.1	− 29.0 ± 0.4	− 27.8 ± 0.3	− 9.6 ± 1.9	36.9 ± 0.5	135.9 ± 4.0
Θ_{ave}(K)	− 61.6 ± 0.8	− 34.7 ± 4.6	− 9.1 ± 0.8	− 7.7 ± 1.0	13.2 ± 3.3	2.5 ± 0.5	32.5 ± 2.8

TABLE II: Anisotropic magnetization values measured at $H = 55$ kG, and the angles α determined as described in the text.

	Tb	Dy	Ho	Er	Tm
M^{exp}([0 0 1]) / $\mu_{sat}(R^{3+})$	0.03	0.69	0.78	0.83	0.33
$\alpha^{(a)}$	88^0	46.5^0	38.6^0	34.0^0	71.0^0
M^{exp}([1 2 0]) / $\mu_{sat}(R^{3+})$	0.68; $0.62^{(b)}$	0.50	0.42	0.28	0.63
α^e; α^h	90^0; 90^0	47.4^0; 51.3^0	39.7^0; 43.8^0	29.1^0; 32.7^0	71.0^0; 73.4^0
α	89.0^0 ± 1.0^0	48.9^0 ± 2.4^0	40.6^0 ± 2.0^0	31.6^0 ± 2.5^0	72.2^0 ± 1.2^0

(a) α values determined using $M([0\ 0\ 1])\ |_{55\ kG}$ (see text).

(b) In-plane anisotropic magnetization values (M^e and M^h) used to calculate the respective α values for TbPtIn.

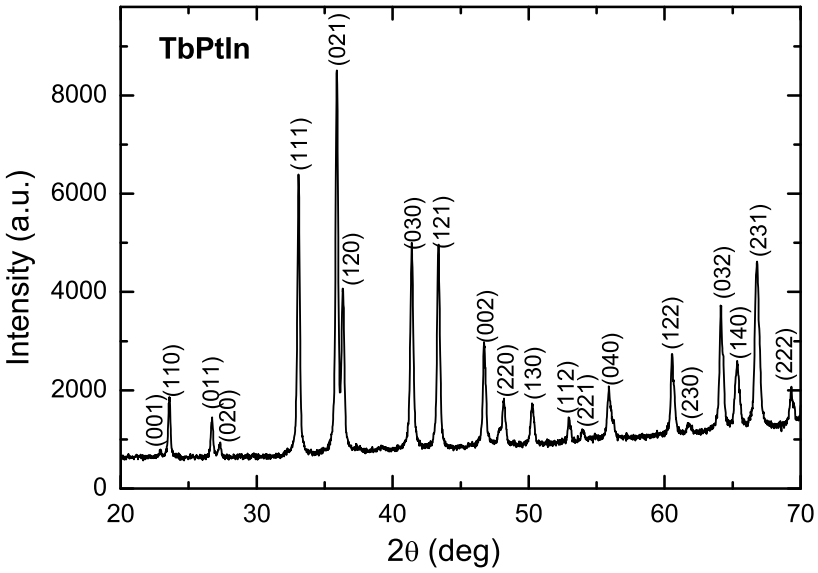

FIG. 1: Powder X-ray diffraction pattern for TbPtIn. All peaks are indexed using a hexagonal P$\bar{6}$2m structure, with $a = 7.56$ $\mathring{A}$ and $c = 3.87$ $\mathring{A}$.

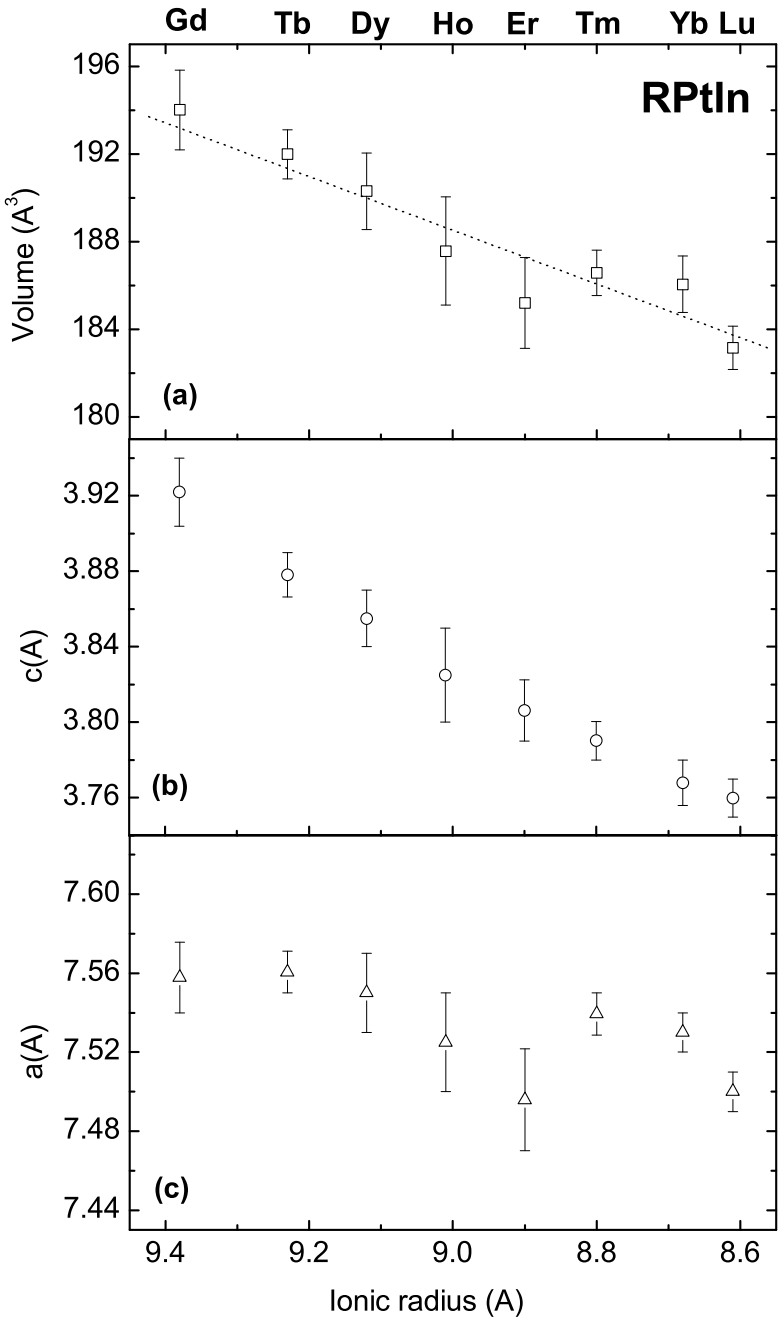

FIG. 2: Unit cell volumes and lattice parameters for RPtIn, R = Gd - Lu, as a function of R^{3+} ionic radius. Dotted line - a guide for the eye, indicating the Lanthanide contraction.

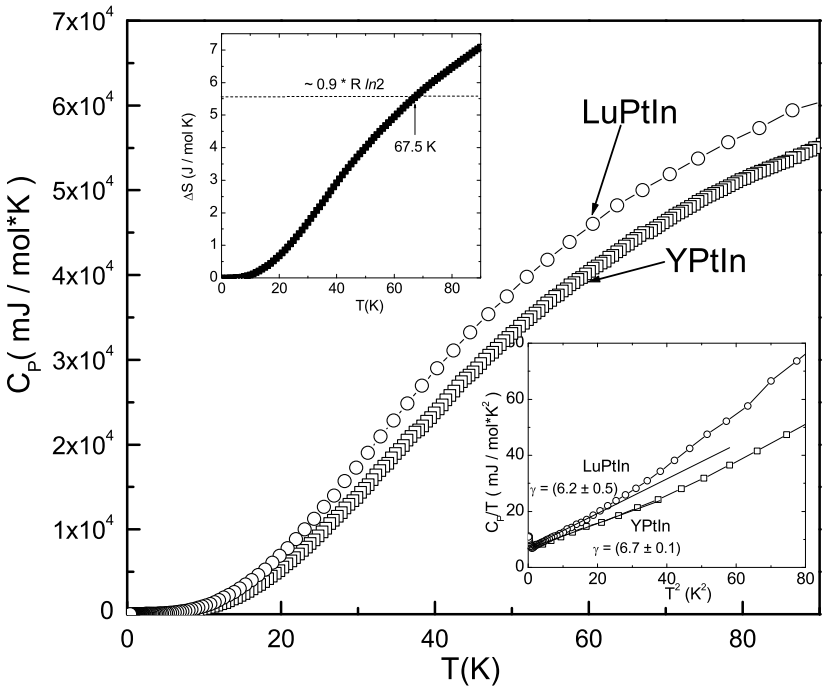

FIG. 3: Heat capacity for YPtIn and LuPtIn, with low-temperature C_P / T vs. T^2 shown in lower inset (linear fits of the low-T data give γ in units of mJ / mol * K^2); upper inset: entropy difference ΔS (see text).

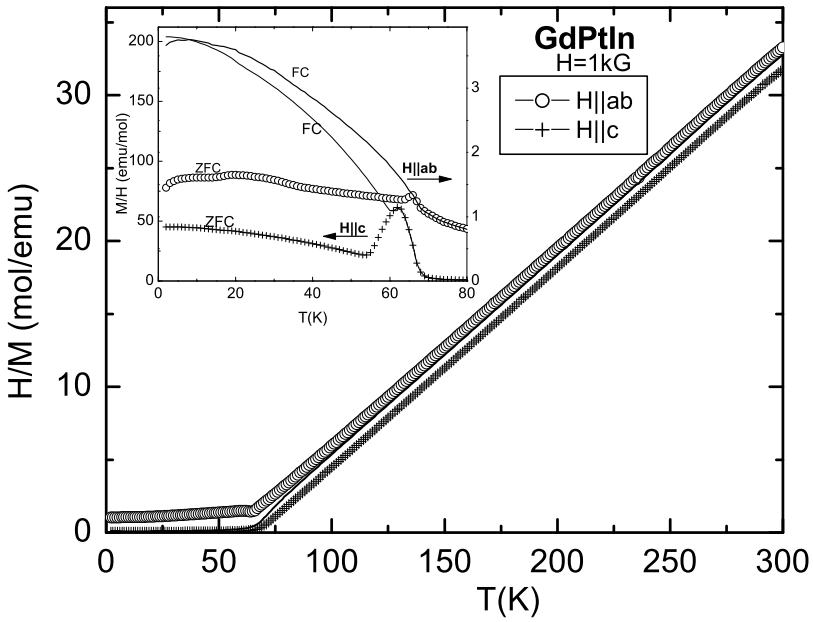

FIG. 4: Anisotropic H / M data of GdPtIn and calculated average (line) at H = 1 kG, with the anisotropic ZFC - FC low-temperature M / H data for H = 0.1 kG shown in the inset.

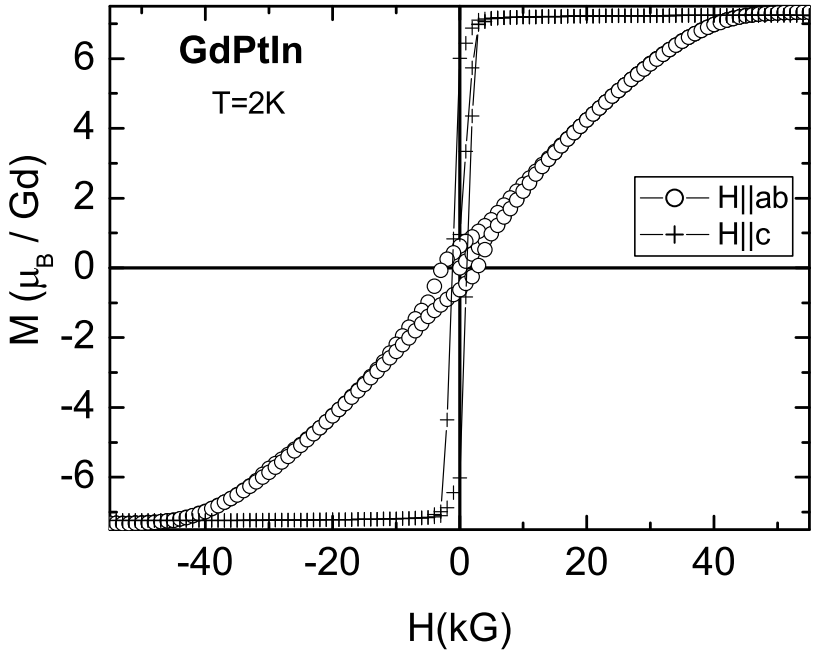

FIG. 5: Anisotropic field-dependent magnetization loops for GdPtIn, at T = 2 K.

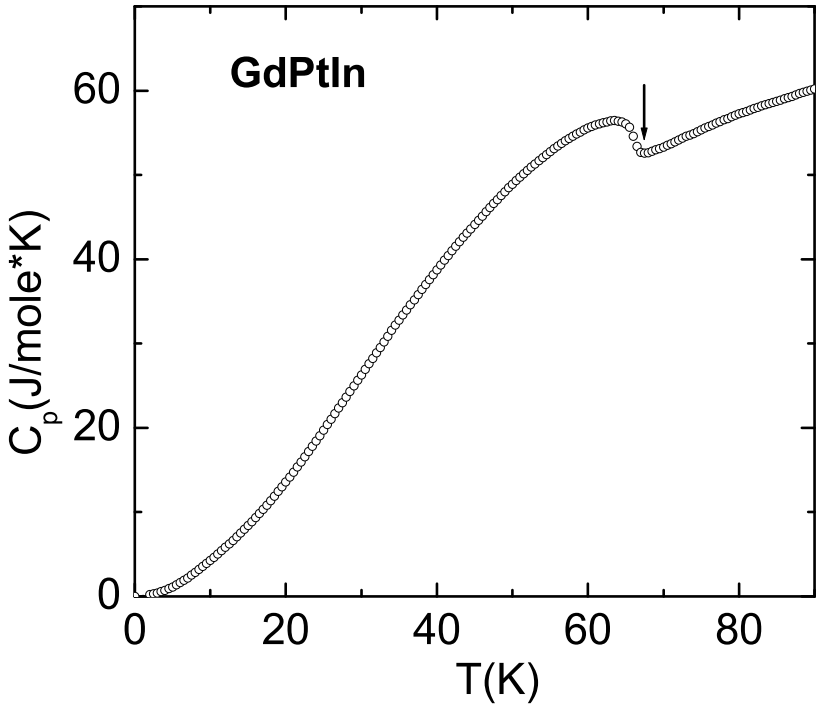

FIG. 6: Specific heat $C_P(T)$ of GdPtIn; small arrow indicates T_C determined from on-set (see text).

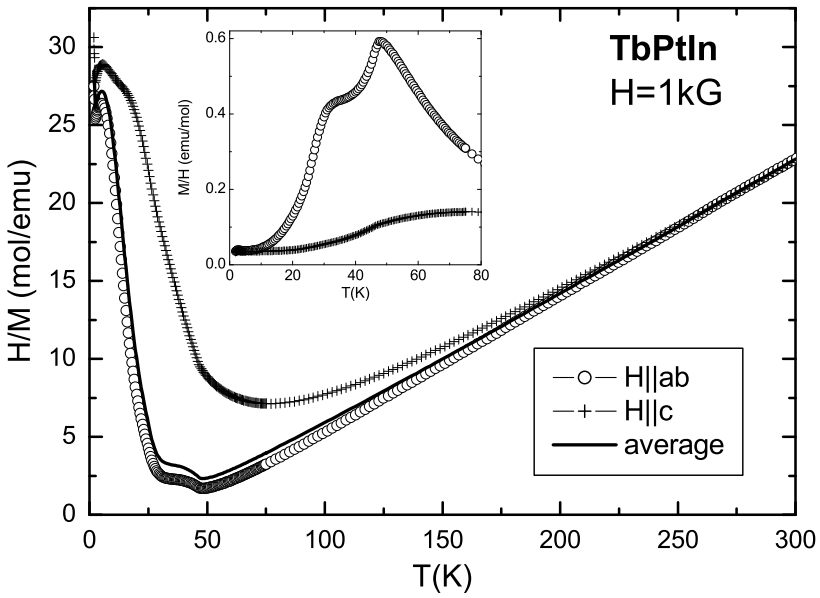

FIG. 7: Anisotropic H / M data of TbPtIn and calculated average (line) at H = 1 kG; inset: low-temperature anisotropic M / H data.

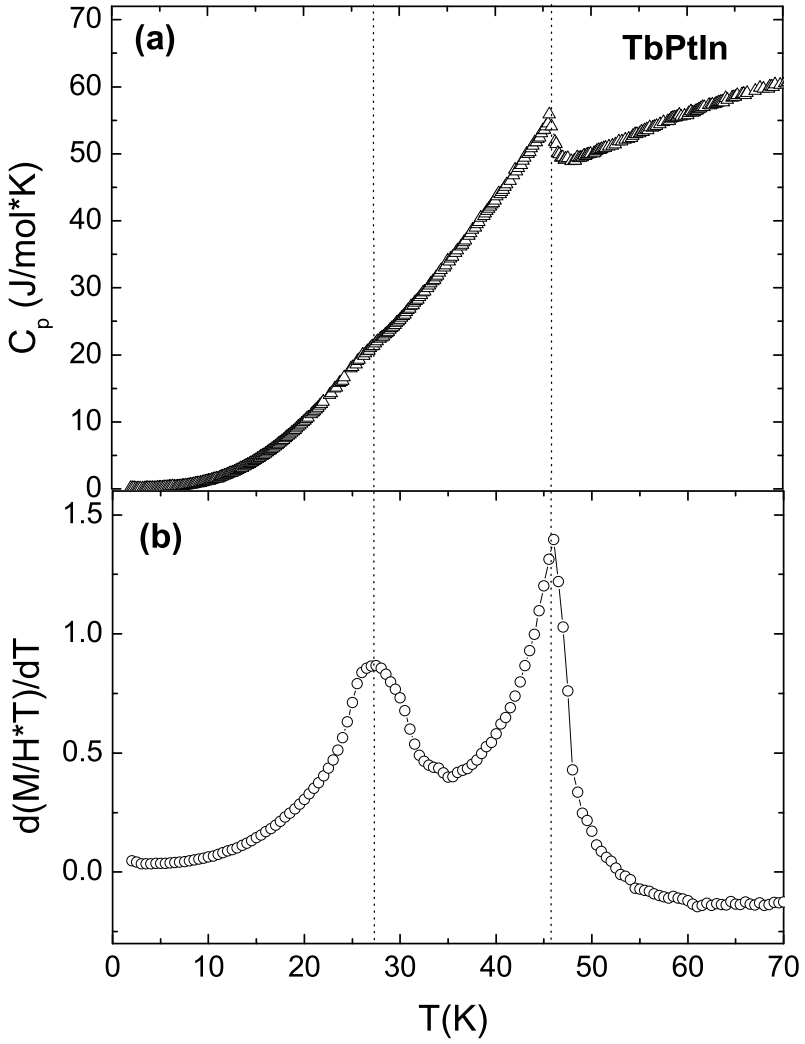

FIG. 8: (a) C_P(T) and (b) low-temperature $d(M_{ave}/H * T)/dT$ for TbPtIn; dotted lines mark the peak positions, corresponding to the magnetic transitions.

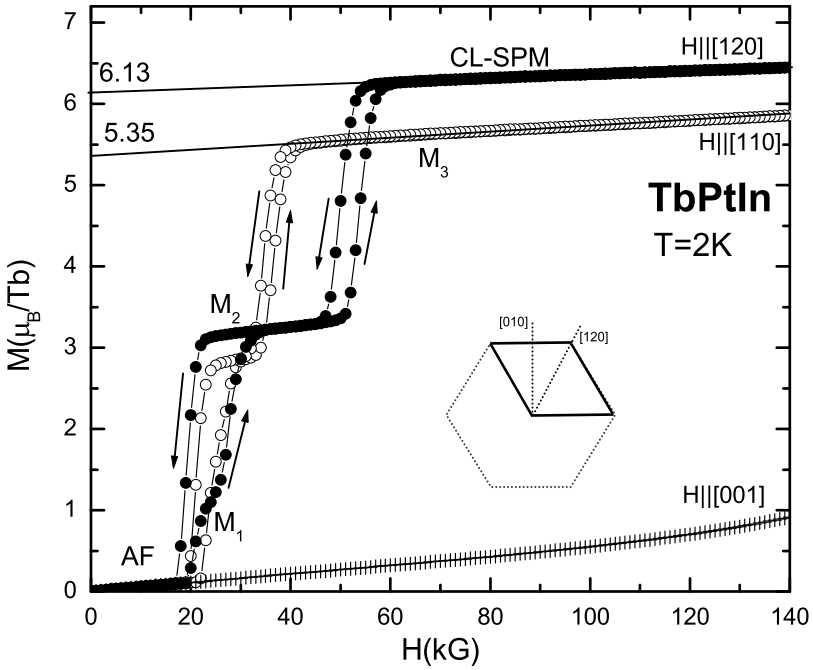

FIG. 9: Anisotropic field-dependent magnetization data for TbPtIn, at T = 2 K, for increasing and decreasing field values (as indicated by arrows).

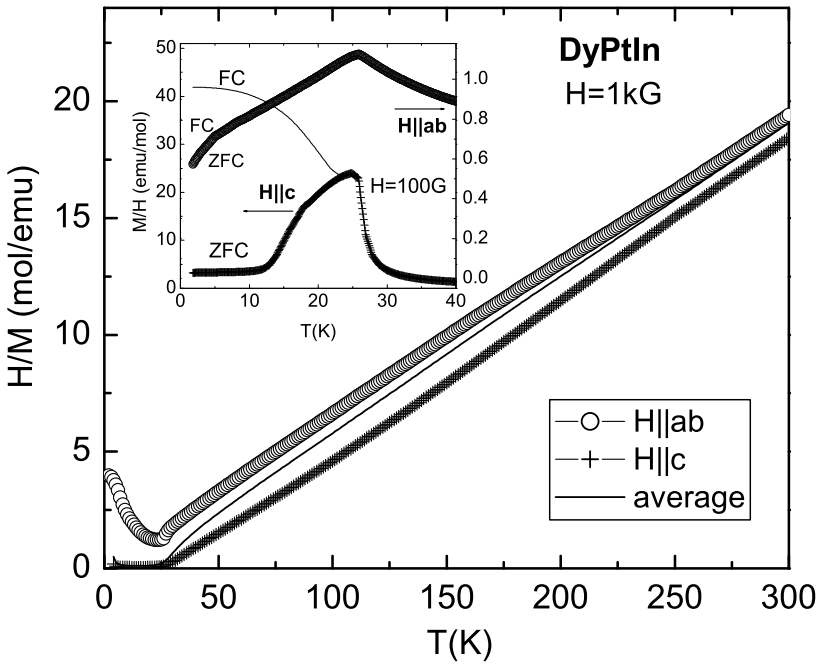

FIG. 10: Anisotropic H / M data for DyPtIn and the calculated average (line) at H = 1 kG; inset: ZFC-FC low-temperature anisotropic M / H data for H = 0.1 kG.

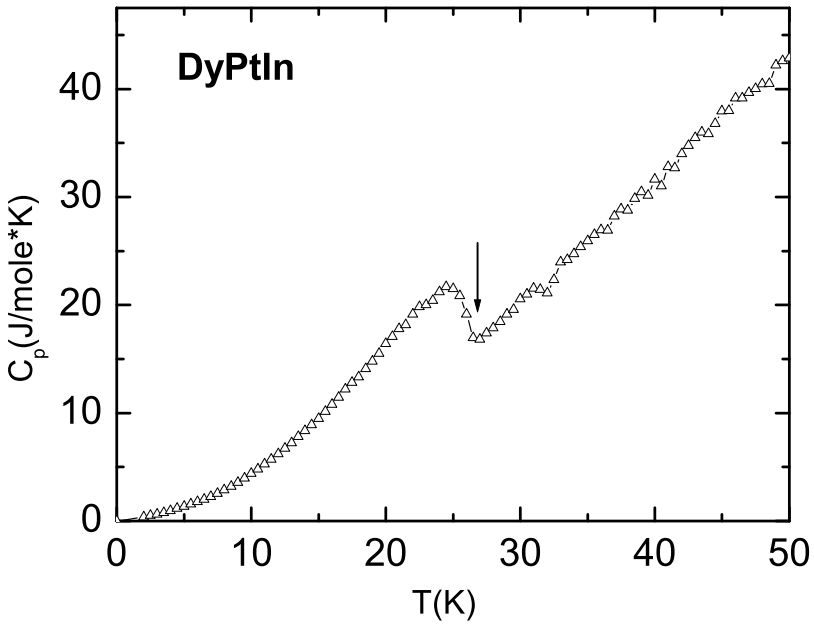

FIG. 11: Specific heat $C_P(T)$ of DyPtIn; small arrow indicates T_C determined from on-set (see text).

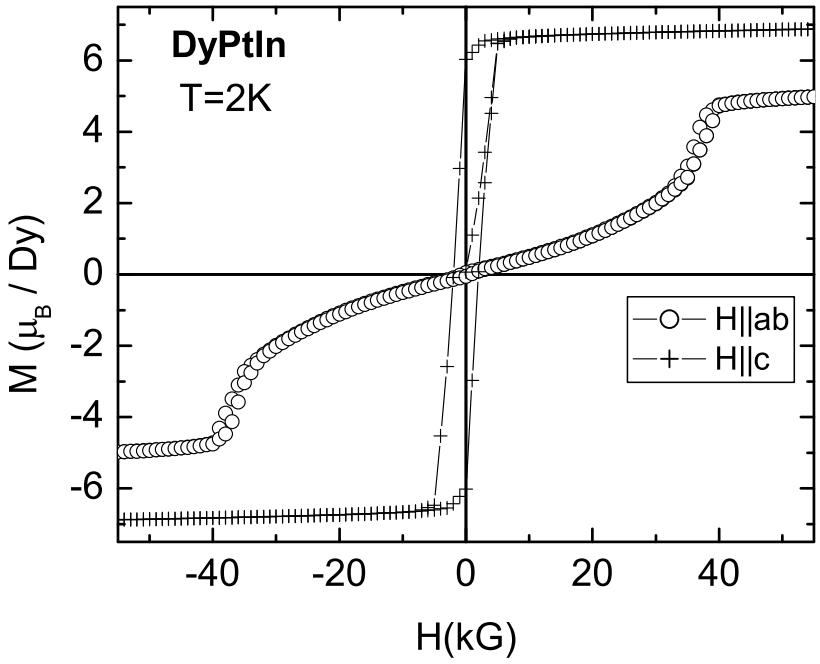

FIG. 12: Anisotropic field-dependent magnetization loops for DyPtIn, at T = 2 K.

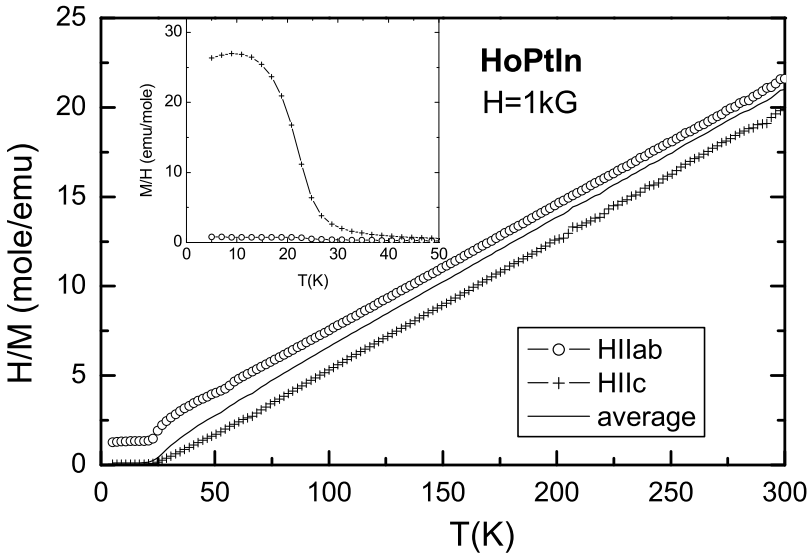

FIG. 13: Anisotropic H / M data for HoPtIn and the calculated average (line) at H = 1 kG; inset: low-temperature anisotropic M / H data.

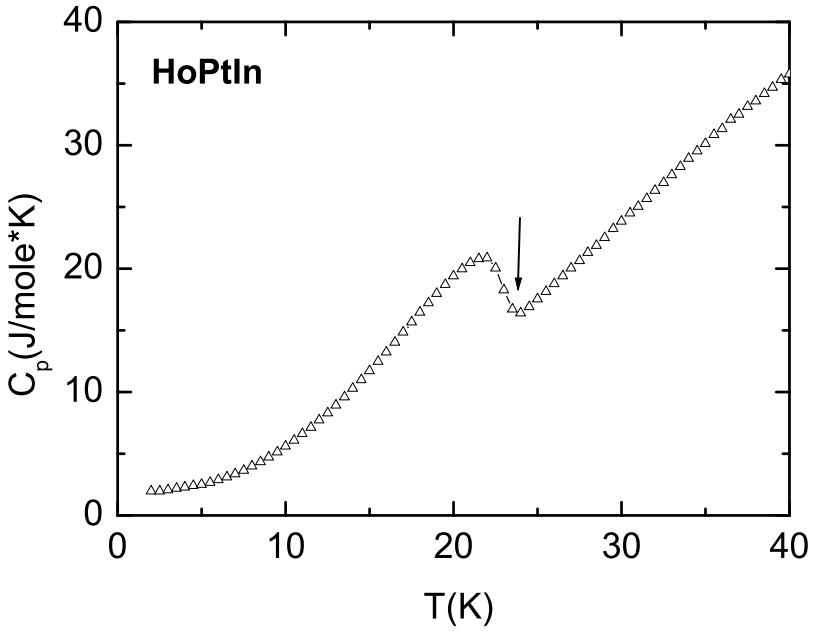

FIG. 14: Specific heat $C_P(T)$ of HoPtIn; small arrow indicates T_C determined from on-set (see text).

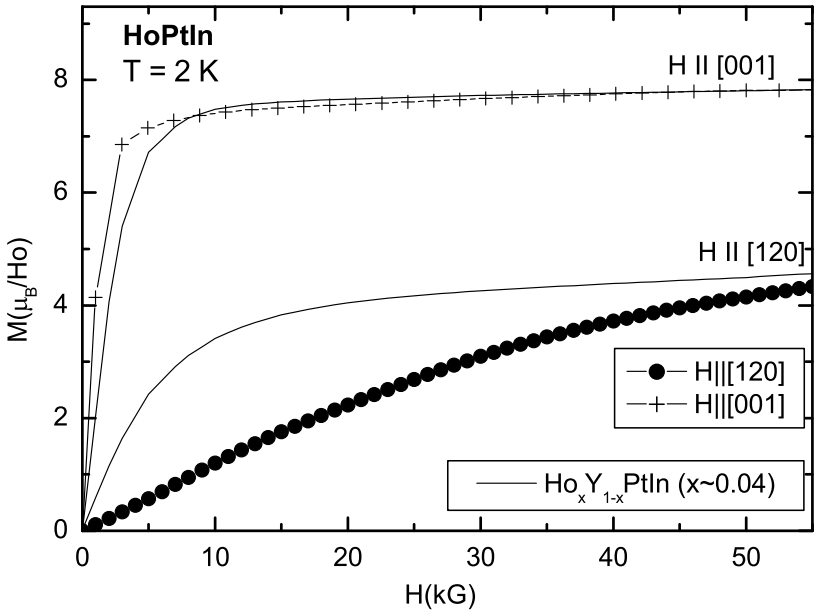

FIG. 15: Anisotropic field-dependent magnetization curves for HoPtIn (symbols), and $Ho_xY_{1-x}PtIn$, x $\sim$ 0.04 (lines), at T = 2 K.

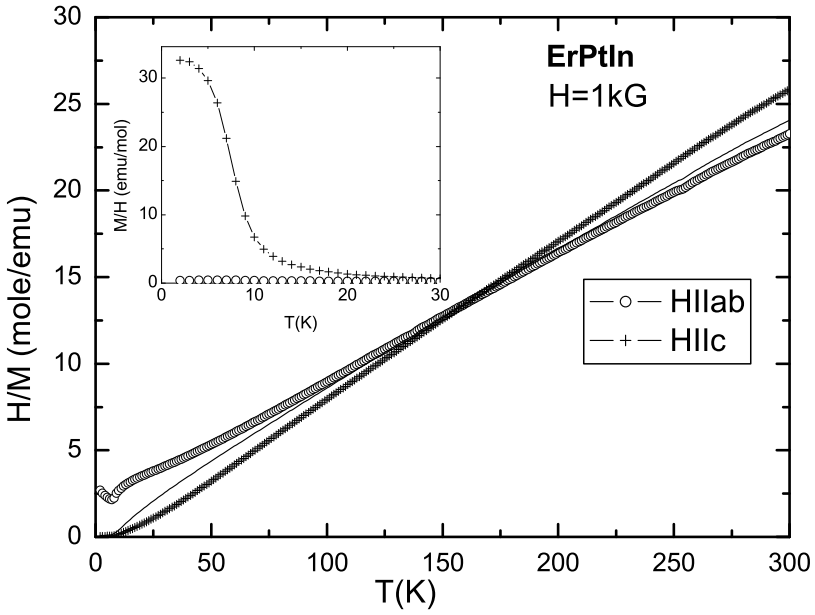

FIG. 16: Anisotropic H / M data for ErPtIn and the calculated average (line) at H = 1 kG; inset: low-temperature anisotropic M / H data.

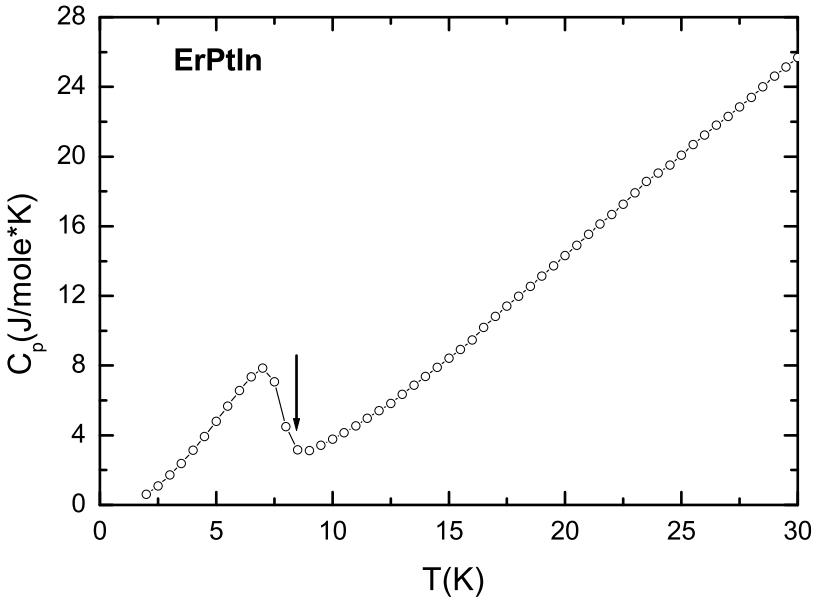

FIG. 17: Specific heat $C_P(T)$ of ErPtIn; small arrow indicates T_C determined from on-set (see text).

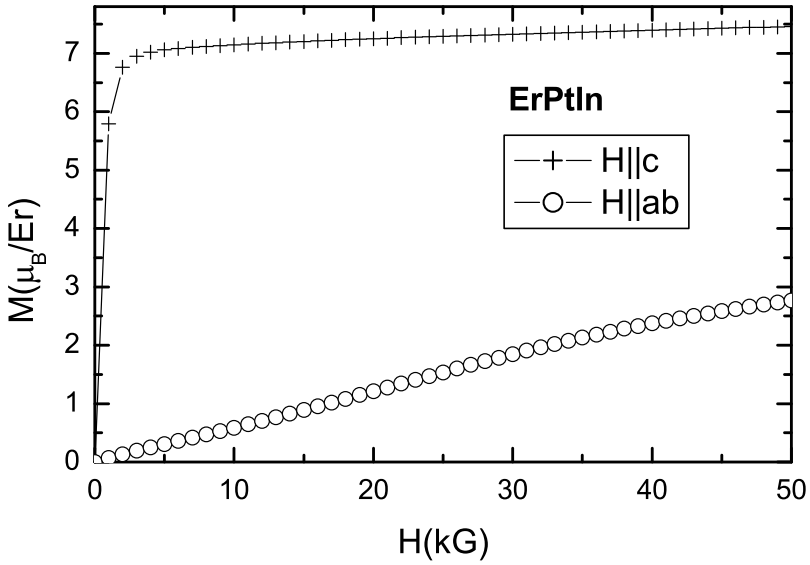

FIG. 18: Anisotropic field-dependent magnetization curves for ErPtIn, at T = 2 K.

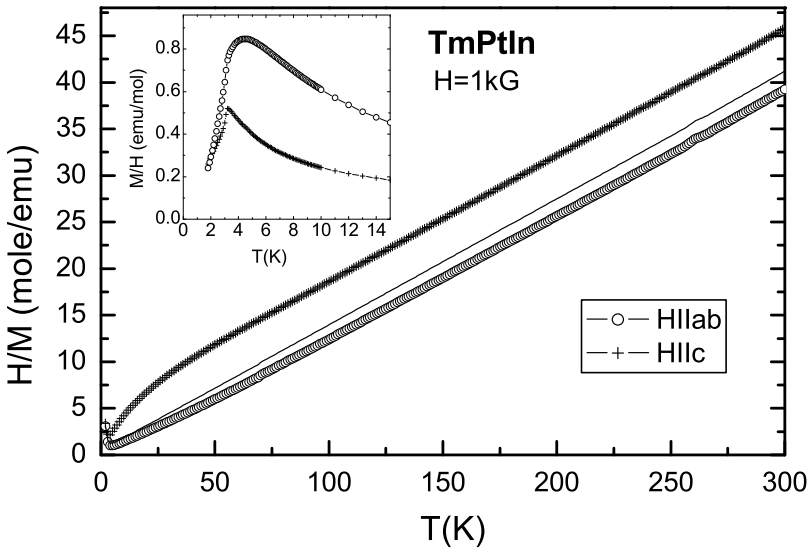

FIG. 19: Anisotropic H / M data for TmPtIn and the calculated average (line) at H = 1 kG; inset: low-temperature anisotropic M / H data.

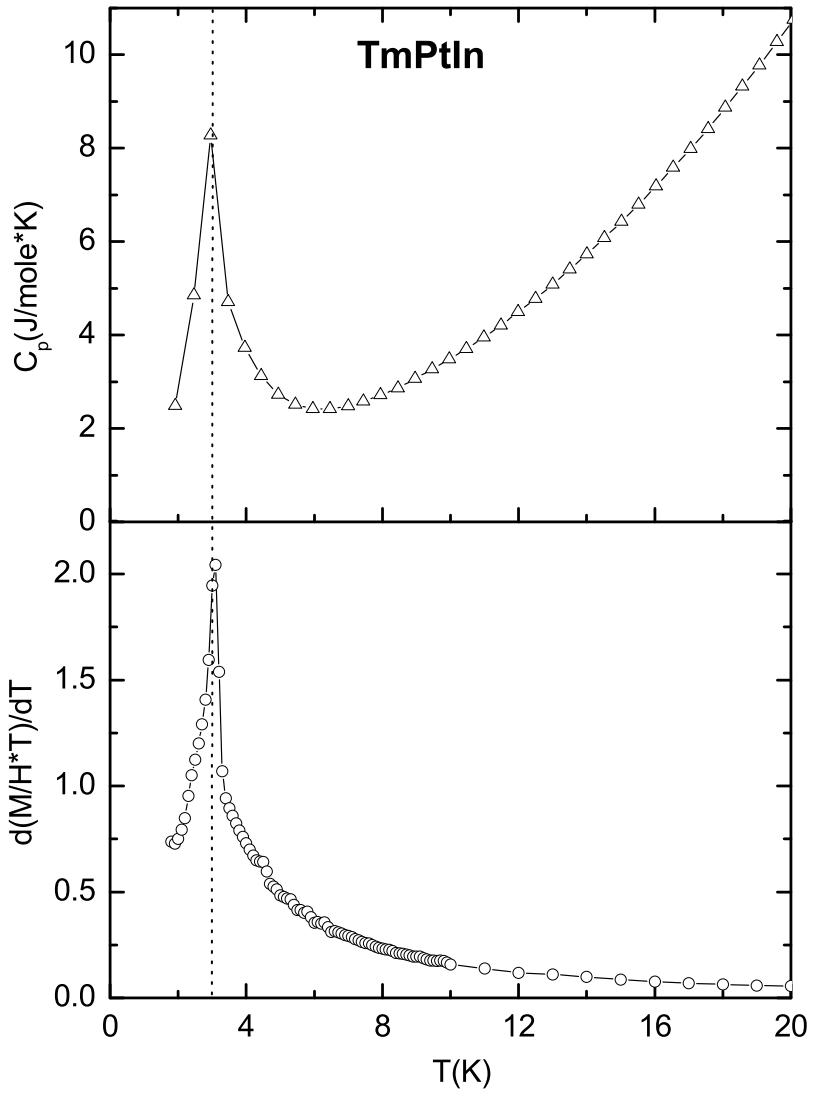

FIG. 20: (a) C_P(T) and (b) low-temperature $d(M_{ave}/H * T)/dT$ for TmPtIn; dotted line marks the peak position, corresponding to T_N.

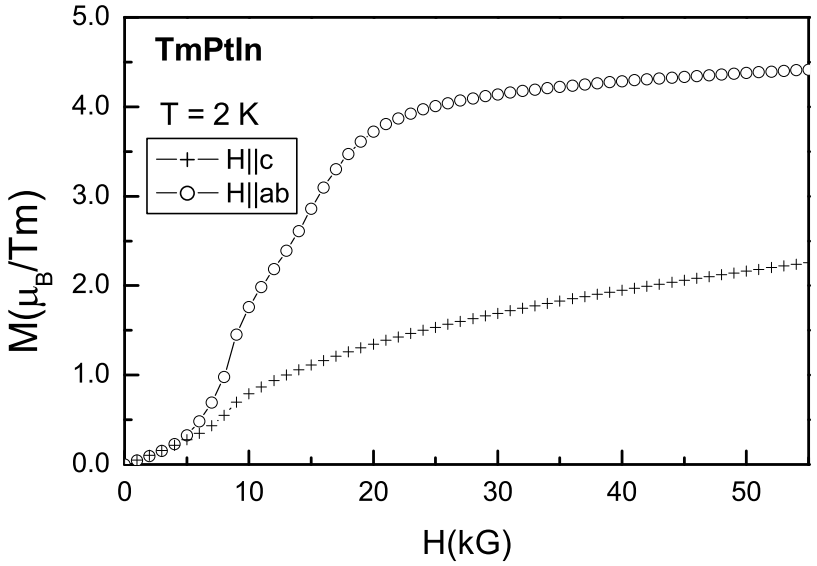

FIG. 21: Anisotropic field-dependent magnetization curves for TmPtIn, at T = 2 K.

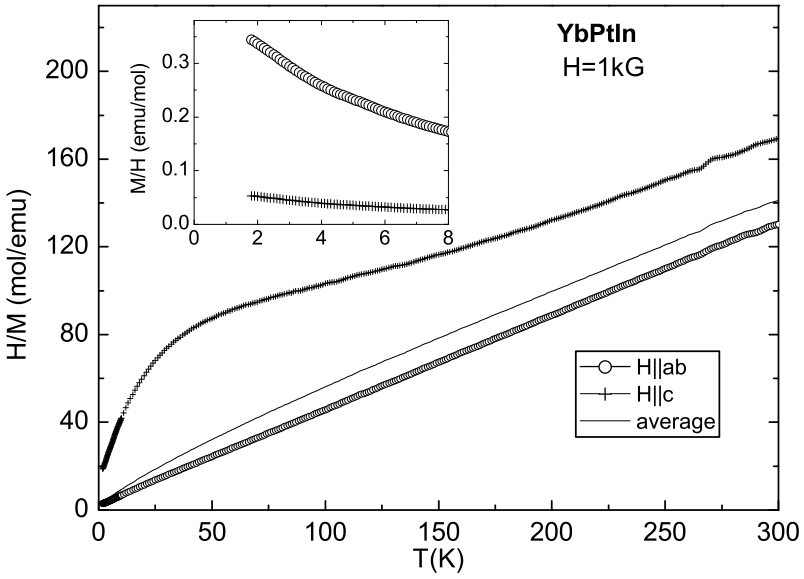

FIG. 22: Anisotropic H / M data for YbPtIn and the calculated average (line) at H = 1 kG; inset: low-temperature anisotropic M / H data.

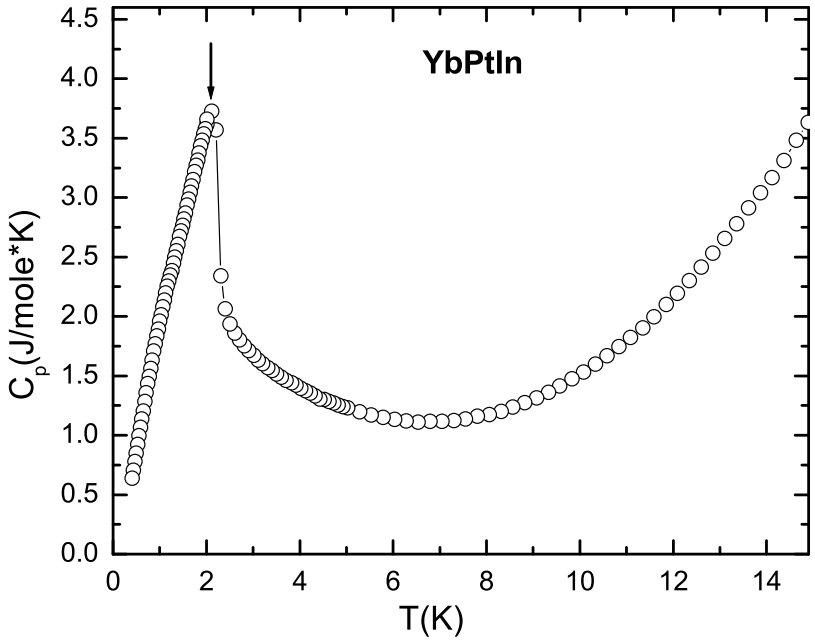

FIG. 23: Specific heat $C_P(T)$ of YbPtIn; small arrow indicates T_m.

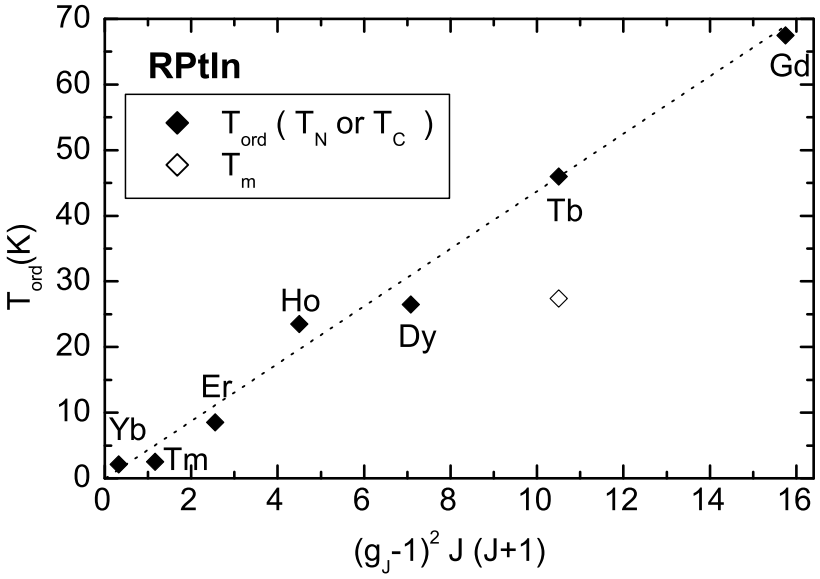

FIG. 24: Changes of the magnetic ordering temperatures T_m for RPtIn (R = Gd - Tm) with the deGennes scaling factor dG (the dotted line represents the expected linear dependence). Open symbol (for R = Tb) represents the low temperature transition from the higher-T to lower-T antiferromagnetic state.

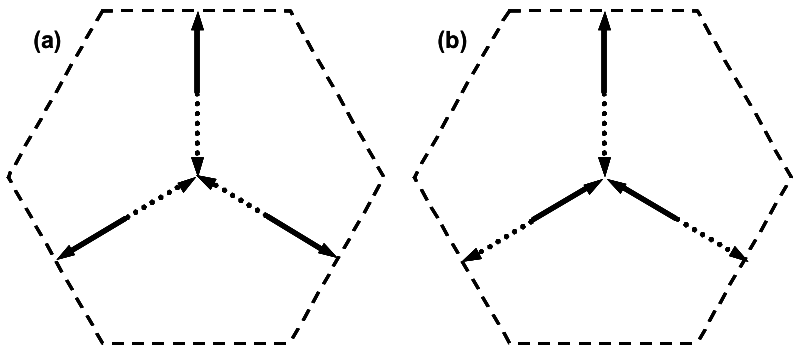

FIG. 25: Schematic representation of the three co-planar Ising-like systems model in (a) the antiferromagnetic and (b) the CL-SPM state. Solid arrows: "up" and dotted arrows: "down" orientations of the magnetic moments along the easy axes.

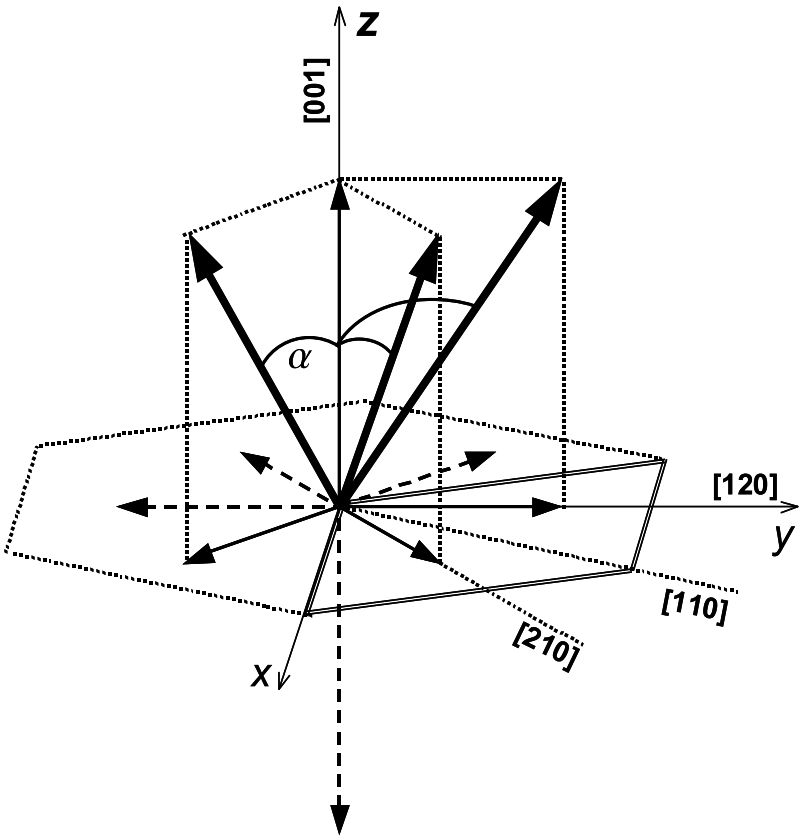

FIG. 26: The three-dimensional model for three magnetic moments at unique orthorhombic point symmetry sites: thin arrows (solid - "up" and dotted - "down") represent the non-zero components of the magnetic moments along the [001] or the easy in-plane directions (as shown, the [120] - equivalent directions). Thick arrows: full magnetic moments in the CL-SPM state.

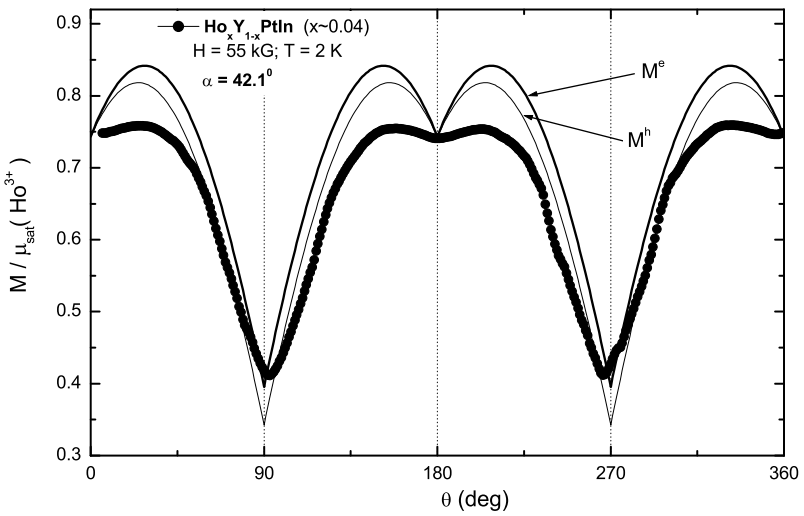

FIG. 27: Angular dependent magnetization for $Ho_xY_{1-x}PtIn$ (x $\sim$ 0.04) (full circles) at H = 55 kG and T = 2 K. The solid lines represent the "easy" and "hard" plane calculated magnetizations as a function of θ (see text), for fixed angle α.